The lncRNA landscape of cardiac resident macrophages and identification of *SchlafenInc* as a regulator of macrophage migratory function

Anne Dueck[1,2], Lara Althaus[1,2], Kathrin Heise[1,2], Dena Esfandyari[1,2], Seren Baygün[3], Ralf P. Brandes[4,5], Julien Gagneur[2,6,7,8], Nicolas Jaé[5,9], Percy Knolle[10], Matthias S. Leisegang[4,5], Lars Maegdefessel[2,11], Thomas Meitinger[2,7], Dierk Niessing[12,13], Niklas Petzold[1,2], Deepak Ramanujam[1,2], Hendrik Sager[2,14], Christian Schulz[2,15], Evangelos Theodorakis[2,6,7,8], Anna Uzonyi[1], Tobias Weinberger[2,15], Ilka Wittig[4,5], Michael Bader[16], Marc Schmidt-Supprian[3], Stefan Engelhardt[1,2]

[1] Institute of Pharmacology and Toxicology, Technical University Munich, Munich, Germany
[2] DZHK (German Centre for Cardiovascular Research), partner site Munich Heart Alliance, Munich, Germany
[3] Institute of Experimental Hematology, Central Institute for Translation Cancer Research, School of Medicine, Technical University Munich, Munich, Germany
[4] Institute for Cardiovascular Physiology, Goethe University, Frankfurt, Germany
[5] DZHK (German Centre for Cardiovascular Research), partner site RheinMain, Frankfurt, Germany
[6] Institute of Informatics, Technical University Munich, Munich, Germany
[7] Institute of Human Genetics, Klinikum rechts der Isar, School of Medicine, Technical University of Munich, Munich, Germany
[8] Computational Health Center, Helmholtz Center Munich, Neuherberg, Germany
[9] Institute for Cardiovascular Regeneration, Goethe University Frankfurt, Frankfurt am Main, Germany
[10] Institute for Molecular Immunology, MRI, Technical University Munich, Munich, Germany
[11] Department of Vascular and Endovascular Surgery, Technical University Munich, Munich, Germany
[12] Institute of Structural Biology, Molecular Targets and Therapeutics Center, Helmholtz Munich, Neuherberg, Germany
[13] Institute of Pharmaceutical Biotechnology, Ulm University, Ulm, Germany
[14] Department of Cardiology, German Heart Centre Munich, Technical University Munich, Munich, Germany
[15] Medizinische Klinik und Poliklinik I, Klinikum der Universität München, Ludwig-Maximilians-Universität, Munich, Germany
[16] Max-Delbrück-Center for Molecular Medicine (MDC), Berlin, Germany

Present address: Anna Uzonyi, Department of Molecular Genetics, Weizmann Institute of Science, Rehovot, Israel

Keywords: long non-coding RNA, cardiac resident macrophages, pressure overload, *SchlafenInc*, single cell sequencing

ABSTRACT

Cardiac resident macrophages (crMPs) were recently shown to exert pivotal functions in cardiac homeostasis and disease, but the underlying molecular mechanisms are largely unclear. Long non-coding RNAs (lncRNAs) are increasingly recognized as important regulatory molecules in a number of cell types, but neither the identity nor the molecular mechanisms of lncRNAs in crMPs are known. Here, we have employed deep RNA-seq and single cell RNA sequencing to resolve the crMP lncRNA landscape from healthy and diseased murine myocardium. CrMPs express previously unknown and highly cell type-specific lncRNAs, among which one lncRNA, termed *Schlafenlnc*, was particularly abundant and enriched in crMPs. We found *Schlafenlnc* to be necessary for migration-associated gene expression in macrophages *in vitro* and *in vivo* and essential for their adhesion and migration. Collectively, our data provide a basis to the systematic characterization of lncRNAs in crMPs and establish *Schlafenlnc* as a critical regulator of macrophage migratory functions.

INTRODUCTION

Long non-coding RNAs (lncRNAs) are the largest group of non-coding RNA molecules, with 14,764 lncRNA genes currently annotated in mouse and 19,933 in humans (Gencode in October 2022). Although only a small fraction of these has been functionally characterized, there is strong evidence that lncRNAs, through a variety of mechanisms, adopt critical roles in disease, for example in cancer[1], metabolic, neurologic[2] and cardiovascular disease[3]. Macrophage lncRNAs in cardiovascular disease have been primarily characterized in the vasculature and within the context of atherosclerosis, e.g., formation of foam cells or polarization (reviewed in [4]). With regard to cardiac disease, the analysis of lncRNAs and their functions has largely focused on cardiomyocytes[5], endothelial cells[6] and fibroblasts[7] (reviewed in [3]). By contrast, very little is known about lncRNAs in cardiac resident macrophages (crMPs), although this cell type constitutes the largest population of immune cells in the myocardium during homeostasis and also determines cardiac disease processes (reviewed in [8]). CrMPs have in recent years been characterized with respect to their developmental origin[9,10], their composition[10,11] and their putative functions such as roles in cardiac conduction[12,13], hypertrophy[14] or lymph vessel growth[15]. Although it can be readily assumed that many of these functions are subject to lncRNA-mediated regulation, a comprehensive description of the lncRNome from crMPs or functional data on a crMP-specific lncRNA is missing thus far.

In this study, we established the first comprehensive analysis of the lncRNA portfolios of the major cardiac cell types in health and disease, with particular emphasis on macrophages. In mouse myocardium, we identified lncRNAs that are specific for, and define, this cell type. One crMP lncRNA that has previously not been analyzed and which we termed *Schlafenlnc*, stands out for its strong enrichment and high abundance in crMPs. Upon functional characterization of a *Schlafenlnc* knockout in a mouse model for left ventricular pressure overload, we found that this lncRNA regulates macrophage abundance in the heart and the ability of this cell type to exert chemotactic migration. We therefore propose that *Schlafenlnc* critically regulates the function of cardiac macrophages in disease.

RESULTS

lncRNAs are important determinants for the definition of specific cell types

To determine the long non-coding RNA (lncRNA) repertoire in the major cardiac cell types and its changes under disease conditions, we subjected mice to chronic left ventricular pressure overload (induced by transverse aortic constriction, TAC), an established model of cardiac inflammation that leads to hypertrophic and fibrotic remodeling of the heart. At day 6 after surgery, we sacrificed the mice, isolated primary cells by Langendorff digestion[16], and performed droplet-based single cell RNA sequencing (scRNA-seq, Chromium platform) (Fig. 1A). This experimental approach analyzes all cardiac non-myocytes, while the number of cardiac myocytes is decreased due to size constraints of the method. Unsupervised clustering of both samples based on the expression of both coding and non-coding RNAs with the Seurat analysis tool (Seurat V3.2[17], Gencode vM22[18]) yielded a total of 20,010 cells after quality control. These comprised all major non-myocyte cardiac cell types (Seurat clustering resolution 0.3, Fig. 1B), including subpopulations of immune cells, fibroblasts, endothelial cells and mural cells (Fig. 1B). Differential gene expression analysis from these cell types revealed distinct sets of protein-coding genes that define each major cardiac cell type as individual clusters (Extended Data Fig. S1), in line with previous reports[19,20].

Despite the generally lower expression levels of lncRNAs in comparison to protein-coding genes[21–24], we were able to readily detect over 440 lncRNAs. Several of the most strongly expressed lncRNAs exhibited a very high level of cell type specificity (Fig. 1C and 1D), suggesting that cardiac cell types can be defined based on their lncRNA transcriptomes. As Fig. 1D shows, our data not only confirmed the previously reported expression of *Meg3* in fibroblasts[25], *H19* in endothelial cells[26] and *Mhrt* in cardiac myocytes[27], but also revealed lncRNAs that had hitherto not been reported to be cell type-specific in the heart. These lncRNAs may reasonably be presumed to potentially exert important roles in their specific cell type, prompting for functional characterization.

To validate the contribution of lncRNAs to cell type identity, we performed differential clustering of the scRNA-seq data sets with or without lncRNA genes, and tested for clustering precision. Independent of whether the top 3,000 variable genes defined by the Seurat pipeline, all annotated genes (n=55,487) or expressed genes (n=19,719, expression value >0) were used to perform clustering, the inclusion of lncRNA marker genes significantly improved clustering compared to protein coding genes alone (Fig. 1E-G). Compared to clustering based on protein-coding genes alone, this resulted in an overall increased sensitivity (indicated by an increased adjusted Rand Index value) and yielded additional subclusters of cell types. Specifically, the detection of clusters representing venous capillary endothelial cells, pericytes, *Fabp4*$^{+}$ macrophages and *Notch2*$^{+}$ fibroblasts was dependent on the inclusion of lncRNAs (resolution 0.65) (Fig. 1H, Extended Data Fig. S1B).

In conclusion, lncRNAs were shown to be a valuable determinant of defining clusters and fine-tuning cell type assignations.

As a means to approach lncRNAs of potential disease relevance, we next thought to assess the expression of lncRNAs during cardiac disease by comparing the datasets obtained from sham-treated vs. TAC-treated mice. Upon increasing the clustering resolution from 0.3 to 0.7, a more detailed and granular cell assignment of lncRNA genes to cellular subtypes was achieved (Extended Data Fig. S2A

113 and S2B). With this setup, we performed differential gene expression analysis for the sub-populations
114 of the major cell types in the heart, and visualized the top de-regulated lncRNAs (Fig. 2A-C, Extended
115 Data Fig. S2C). Some lncRNAs were regulated after TAC throughout all subpopulations of a cell type,
116 e.g., Gm29686 in fibroblasts (Fig. 2A), whereas others were only significantly regulated within a defined
117 subpopulation, e.g., Gm49785 in the fibroblast subpopulation (FB6) (Fig. 2A). This subpopulation of
118 fibroblasts represents activated myofibroblasts (high expression of periostin), a cell type involved in
119 extracellular matrix secretion and immune cell recruitment[28]. Similarly, several lncRNAs displayed
120 dysregulation within cardiac endothelial cells (Fig. 2B) and cardiac macrophages (Fig. 2C), resolved to
121 the level of cellular subtypes.
122 Of particular interest are lncRNAs in macrophages of the myocardium, since no lncRNA had thus far
123 been identified or functionally characterized in this cardiac cell type. As a first approach to the potential
124 function of the lncRNAs we had identified as deregulated in crMPs in the TAC model, we correlated
125 these lncRNAs with biological processes of their overlapping neighboring genes (Extended Data Fig.
126 S2D). Since lncRNAs are often co-expressed and co-regulated with proximal genes in *cis*[29], we
127 speculated that the latter may give insight into the biological context within which these lncRNAs
128 function. For example, genes antisense to downregulated lncRNAs in the Mac1 cluster (*Lyve1*
129 macrophages) after TAC are associated with programmed cell death processes and genes antisense
130 to downregulated lncRNAs in the Mac2 cluster (*Cd74*+ macrophages) after TAC were predominantly
131 linked to adhesion pathways (Extended Data Fig. S2D), suggesting that the reported de-regulated
132 lncRNAs might also be involved in the regulation of these processes.
133 Taken together, we report a comprehensive inventory of regulated lncRNA genes in the major non-
134 myocyte cell types of the heart during pressure overload. These lncRNA genes will be interesting
135 candidates to be studied in more detail.

136 **Determination and annotation of the lncRNA landscape of cardiac resident macrophages**

137 As the sequencing depth of current single cell sequencing methodology limits detection sensitivity, we
138 therefore complemented our scRNA-seq data by performing deep RNA-Seq on basal total murine
139 myocardium as well as crMPs that were isolated using well-established cell markers (CD45, CD64,
140 CD11b and F4/80[9,10]). These surface proteins collectively labelled essentially all crMPs in our scRNA-
141 seq data (Extended Data Fig. S3A), corroborating our purification strategy. Using a pipeline to identify
142 and quantify novel lncRNAs (Extended Data Fig. S3B), we identified 250 genes that had previously not
143 been annotated by Gencode vM22[18]. The identified novel lncRNAs showed the same characteristics as
144 the known lncRNAs with respect to having no coding probability (true non-coding) and transcript length
145 (Extended Data Fig. S3C upper panel), but were more highly expressed in our data set than the known
146 lncRNA population (Extended Data Fig. S3C lower panel). RNA-seq from fractionation experiments
147 showed for known lncRNAs a distribution of 80% in the nucleus (and 20% to the cytoplasm), the novel
148 lncRNAs are slightly less nuclear in localization (70% nuclear, 30% cytoplasmic; Extended Data Fig.
149 S3D).
150 As a further approach to the function of the newly identified lncRNAs, we built on the observation that
151 the products of lncRNA genes and protein-coding genes which are in proximity of 5kb or less and in
152 antisense overlapping orientation are prone to interact in the same biological processes[30]. The

153 distribution of the interaction categories (e.g. “antisense overlapping”) was comparable between novel
154 and known lncRNAs (Extended Data Fig. S3E). Notably, 15 novel lncRNA genes were found without
155 any interaction, categorizing them as novel long intergenic RNAs (lincRNA). For both known and novel
156 lncRNAs we found many well-expressed genes (> 5 transcripts per million reads, TPM) that are specific
157 in cardiac macrophages compared to total murine myocardium (containing myocytes, endothelial cells,
158 fibroblasts, and macrophages) (Fig. 3A).

159 **Identification of lncRNA *SchlafenInc* as an abundant and enriched macrophage lncRNA**

160 In order to select lncRNA candidates for experimental validation, we further filtered the datasets from
161 scRNA-Seq data and RNA-Seq based on the following stringent criteria: low coding probability
162 according to CPAT score (true non-coding RNA < 44% coding probability), absolute expression > 25
163 TPM in macrophages, enrichment of log2FC >3 and FDR <0.05, and de-regulation in TAC (scRNA-seq
164 data) FC >0.25). This yielded 13 lncRNA candidates that are highly abundant, enriched and regulated
165 in cardiac macrophages (Fig. 3B).

166 We found one of these candidates, lncRNA *AI662270*, particularly interesting due to its genomic
167 association with a cluster of eight genes on chromosome 11 which encode members of the Schlafen
168 family of proteins (Fig. 3C). Schlafen proteins are found in human and mouse and known to regulate
169 important processes and functions such as immune cell development, invasion and migration[31].
170 *AI662270*, however, is a hitherto uncharacterized gene within this locus. The genomic location of
171 lncRNA *AI662270* in the Schlafen cluster led us to name the transcript *SchlafenInc.*

172 The Schlafen locus of protein-coding genes is very similar between human and mouse in general,
173 yet the internal order of the proteins (and lncRNAs) is slightly different. A study by Ulitsky and colleagues
174 developed a pipeline to identify syntenic genes across multiple organisms, where lncRNAs are tested
175 on the relative location and orientation to orthologous protein-coding genes[32]. By comparing Gencode
176 annotations[18] of human (V30) and mouse (vM21) with their pipeline, the gene *ENSG00000267074* was
177 designated as the putative human *SchlafenInc* homolog (Fig. 3C). It is expressed in various human cell
178 types of leukocyte origin (using the RNA-Get module Encode data sets[33], Extended Data Fig. S4A),
179 making it an attractive molecule for studying the observed phenotypes in human cells. Besides the
180 analysis of expression, we tested if the two lncRNAs share common potential binding partners using a
181 pretrained deep neural network (DNN)[34] on eCLIP-seq data[35]. Indeed, the mouse *SchlafenInc* and
182 human *ENSG00000267074* contain three major binding modules of the same or similar proteins
183 (Extended Data Fig. S4B and S4C), supporting the hypothesis of conservation.

184 Murine *SchlafenInc* was up-regulated after TAC in both macrophage populations, but even more
185 pronounced in Mac2 (*MHCII*-high, *Cd74*+) macrophages (Fig. 3D). Its strong expression made it readily
186 detectable by Northern blotting (Fig. 3E). Interrogation of the RNA-seq datasets from the nucleus and
187 the cytosol, as well as RNA *in situ* hybridization, showed that *SchlafenInc* localizes to both compartments
188 (Fig. 3F and G, Extended Data Fig. S4D).

189 ***SchlafenInc* determines myocardial macrophage infiltration and polarization in response to**
190 **pressure overload**

191 To assess the phenotype of a macrophage-specific deficiency of *SchlafenInc in vivo*, we generated a
192 *SchlafenInc*-deficient mouse line (*SchlafenInc*$^{-/-}$) by CRISPR/Cas9 and examined these mice under
193 basal and disease conditions. The dominant transcript was targeted with specific sgRNAs, including the
194 promoter region upstream of *SchlafenInc* (determined by H3K4me3 signals in murine bone marrow-
195 derived macrophages, ENCODE data set ENCSR000CFF[36]) to abrogate all transcription from that locus
196 (Extended Data Fig. 5 A). Deletion was verified by PCR from genomic DNA (Extended Data Fig. 5 B).
197 The early compensation stage of the TAC model is characterized by sterile inflammation and both an
198 influx of monocytes as well as proliferation of resident macrophages. We therefore performed sham and
199 TAC surgery (Fig. 4 A) and analyzed the heart phenotype and monocyte/macrophage numbers after 6
200 days (Fig. 4 B). The heart weight of *SchlafenInc*-deficient mice was significantly reduced (Fig. 4 C) and
201 heart function (comparing ejection fraction of sham and TAC mice) was significantly improved (Fig. 4
202 D). Furthermore, *SchlafenInc*$^{-/-}$ hearts showed a substantial decrease in pressure overload-induced
203 interstitial fibrosis (Fig. 4 E) and interestingly a significantly reduced monocyte/macrophage infiltration
204 after TAC, as determined by immunostaining of left ventricular myocardial sections against the
205 monocyte/macrophage marker CD68 (Fig. 4 F).

206 To assess the composition of immune cells in more detail we next performed scRNA-seq of the CD45+
207 cell fraction isolated from the myocardium and blood (Fig. 5 A). As expected, macrophages are the
208 dominant cell population within the heart whereas the blood contains more monocytes (Fig. 5 B).
209 Activated macrophages and monocytes release signals in an auto- and paracrine fashion[19].
210 *SchlafenInc*$^{-/-}$ mice showed decreased signaling between almost all macrophage and monocyte
211 populations after 6 days of TAC (Fig. 5 C), with a significant decrease in inflammatory signaling
212 pathways such as Osteopontin (*Spp1*) and Macrophage Inhibitory Factor (*Mif*) signaling (Fig. 5 D), both
213 are important factors in recruiting monocytes and other inflammatory cells from the blood after cardiac
214 injury[37,38]. Performing RNA velocity analysis of cardiac leukocytes after TAC (Fig. 5 E) showed gene
215 dynamics of *SchlafenInc* WT *Ly6C*-high monocytes towards non-classical monocytes as well as a
216 moderate dynamic from *MHCII*-high macrophages to *Lyve1* macrophages. In
217 *SchlafenInc*$^{-/-}$, the dynamics between different monocyte states was largely abolished while transition
218 dynamics from monocyte-derived macrophages (*MHCII*-high) to resident-like macrophages (*Lyve1*) was
219 strongly increased (Fig. 5 E). Taken together, the analysis of *SchlafenInc*$^{-/-}$ myocardium indicated
220 stronger polarization of cardiac macrophages towards the *Lyve1* macrophage population, which is
221 generally believed to play a more anti-inflammatory role in disease.

222 Next, we asked which genes were changing globally in *Lyve1* macrophages after TAC and upon
223 *SchlafenInc* deletion. Among the genes that were de-regulated during TAC (WT TAC vs. sham), 64
224 genes were additionally strongly de-regulated in *SchlafenInc*$^{-/-}$ vs. *SchlafenInc* WT *Lyve1* macrophages
225 (|Log2FC|>0.5, FDR<0.05). 17 of these genes are classified as coding for secreted proteins (Fig. 5 F,
226 categorization according to Human Protein Atlas[39]), for example, *Lgals3* (Galectin-3) and *Spp1*
227 (Osteopontin), which were de-regulated in all macrophage populations (Extended Data Fig. 5 C). An

228 analysis of the associated biological processes of de-regulated genes in *Lyve1* macrophages (Fig.5 F)
229 showed leukocyte chemotaxis and migration as the strongest impacted pathways (Fig. 5 G).

230 Taken together, *SchlafenInc* deletion in immune cells of the heart altered the cardiac macrophage
231 response to early pressure overload towards an anti-inflammatory phenotype and disease-associated
232 phenotypes such as fibrosis and heart weight were improved.

233 ***SchlafenInc* is required for macrophage adhesion and migration**

234 To elucidate the function of *SchlafenInc* in more detail and explore its potential role in migration
235 processes, we generated *SchlafenInc*-deficient macrophages from Hoxb8-FL macrophage
236 progenitors[40,41] (Extended Data Fig. S6A). Gene deletion was validated by RNA-Seq (Extended Data
237 Fig. S6A, middle track). As a genomic deletion might have an impact on nearby genes due to a
238 mechanism in *cis* by the deleted lncRNA or due to the deletion of a regulatory element within the DNA,
239 the surrounding region of *SchlafenInc* (0.5 Mbp in each direction) was analyzed for de-regulation
240 (Extended Data Fig. S6B). 9 of 64 genes were found to be moderately dysregulated (with |log2FC| > 1,
241 FDR < 0.05) in the vicinity of *SchlafenInc* revealing that there was not a general activation or de-
242 activation of that locus by *SchlafenInc*. To identify major perturbations on gene expression level,
243 *SchlafenInc*-deficient monoclonal cell lines (2 clones, each measured in n=4) were subjected to RNA-
244 Seq. These samples were compared to control monoclonal cell lines (two clones with n=3 each) that
245 were generated using an unrelated sgRNA (sequenced as wildtype at the *SchlafenInc* locus). We
246 observed 2,660 genes significantly de-regulated (|log2FC| > 1, FDR < 0.05) (Fig. 6 A), among those
247 *SchlafenInc* that dropped from 67 TPM to 0.33 TPM. Among the downregulated genes, we observed an
248 enrichment of genes involved in migration and adhesion similarly to our *in vivo* study (Fig. 6 B, e.g.,
249 *Mmp14* and *Lgals3*). Lower amounts of *Lgals3* could not only be observed in our RNA-Seq data but
250 were validated on protein level (Galectin-3 is the gene product of *Lgals3*) by measurement of cell culture
251 supernatant using an enzyme-linked immunosorbent assay (ELISA) (Fig. 6 C). More generally, gene
252 ontology analysis of all significantly de-regulated genes implicated pathways such as regulation of
253 cytokine production, regulation of cell adhesion and chemotaxis that are promoted by *SchlafenInc* (Fig.
254 6 D). To validate these results, we performed an adhesion assay by rigorous washing (Fig. 6 E) as well
255 as tested the chemotactic migration ability of *SchlafenInc*-deficient macrophages with a gradient of the
256 chemokine C5a (Fig. 6 F). Adhesion was diminished by approximately 23% (Fig. 6 E) and chemotaxis
257 was about 50% reduced (Fig. 6 F) in *SchlafenInc* KO cells compared to wild type controls.
258 To identify interaction partners of SchlafenInc that might contribute to this observed phenotype, we
259 performed a streptavidin pulldown using lysates from bone marrow-derived macrophages incubated
260 with a biotin-labelled SchlafenInc RNA probe (Extended Data Fig. S6C). The subsequent mass
261 spectrometry analysis identified 27 proteins which significantly bound to SchlafenInc, with the top
262 enriched proteins being PURA and PURB (Extended Data Fig. S6D). PURA (purine-rich element binding
263 protein A) and PURB (protein B) are Pur family members essential for DNA replication, gene expression,
264 and cell growth (reviewed in [42]). Both bind purine-rich DNA and RNA sequences, thereby modulating
265 transcription and mRNA stability, can function independently or as a heterodimer[43,44] and are also known
266 to interact with lncRNAs to regulate gene expression[45]. Next, we validated the interaction with PURA

using a specific monoclonal antibody against PURA[44] and indeed could show significant enrichment of SchlafenlnC after immunoprecipitation of PURA (Extended Data Fig. S6E and F). As a known transcriptional regulator, PURA might therefore be involved in the gene expression changes caused by SchlafenlnC, but further studies are required to elucidate this mechanism.

Together these data obtained on *SchlafenlnC*-deficient macrophages corroborate a cell autonomous role for this lncRNA in macrophages, in line with its specific expression in this cell type. *SchlafenlnC* is required for the activation of macrophage gene programs underlying cell adherence and migration providing a mechanistic basis for the phenotype observed *in vivo* in *SchlafenlnC*-deficient mice.

DISCUSSION

This study provides the first comprehensive lncRNome of cardiac resident macrophages. One of the most highly enriched and abundant lncRNAs in cardiac resident macrophages – lncRNA *AI662270*, which we termed *SchlafenlnC* – was shown to be involved in adhesion and migration. As for *SchlafenlnC*, a particular characteristic of lncRNAs in general is their high degree of cell type-specificity[21–23] which makes them important for processes such as development, differentiation of cell types, cellular fate and function (reviewed in [3]). This characteristic could therefore make lncRNAs the natural choice when describing cell population expression signatures, especially in single cell RNA sequencing (scRNA-seq). scRNA-seq allows for an unbiased approach to identify main- and sub-populations of cells, yet little focus has been set to expressly include lncRNA marker genes. Initially, methodical problems such as library preparation, sequencing depth or analysis software hampered the detection of lncRNAs in such data sets. LncRNAs are still not as readily measured as mRNAs due to their on average lower expression levels, but together with improved scRNA-seq depth and improved annotations, our data suggest that lncRNAs are underestimated markers of cell type definition. Emerging platforms measuring RNA transcripts in tissue such as spatial transcriptomics or *in situ* sequencing (reviewed in [46]) might be able to leverage that potential further.

Focusing on lncRNAs and their potential regulation in ventricular myocardium during disease, we could identify an extensive set of regulated lncRNAs for all major cell populations. In general, we find more up-regulated than down-regulated genes upon induction of disease, which we believe to be due to the detection limit of scRNA-seq concerning very lowly expressed genes[47]. LncRNAs more specific to and regulated in a subset of cell types might offer new possibilities for therapeutic intervention and to gain insight into regulatory mechanisms specific for defined cell types. As we have shown for the three macrophage clusters (Mac1 (*Lyve1*+), Mac2 (*Cd74*+) and transitional macrophages), the different sets of regulated lncRNAs are implicated in distinct gene ontology pathways, which points to distinct functions of these macrophage populations.

Cardiac resident macrophages have been shown to be key players in diseases such as heart failure and myocardial infarction (reviewed in [48–51]). In the mouse model of left ventricular pressure overload, crMPs are proliferating during the compensation phase (from 0 days to about 7-14 days). An infiltration of monocyte-derived MPs starts early in disease and increases in the late, decompensated phase[52]. The infiltration of monocyte-derived MPs is typically associated with a long-term detrimental cardiac function[52–59]. This recruitment of monocytes is at least to some degree dependent on crMPs[60], and suppression of this communication axis might be beneficial. Galectin-3, for example, is known to be

308 increased in heart failure patients[61] and is associated with murine cardiac remodeling during pressure-
309 overload[62]. It is well known to be involved in the monocyte as well as macrophage migration and
310 infiltration in cardiovascular diseases[63–65]. Our combination of unbiased scRNA-seq measurements and
311 in-depth coverage by RNA-Seq allowed us to identify the hitherto uncharacterized lncRNA *Schlafenlnc*
312 as a regulator of macrophage adhesion and migration. *Schlafenlnc* is up-regulated after 6 days of TAC
313 as well as other genes involved in adhesion and migration such as Galectin-3 and its deletion impacts
314 Galectin-3 expression both *in vivo* and *in vitro*. Our quantitative assessment of macrophage/monocyte
315 numbers (CD68 staining) and the analysis in relative immune cell composition by scRNA-seq after 6
316 days of TAC point to a mechanism of defective signaling by *Schlafenlnc*-deficient crMPs to initiate
317 recruitment of inflammatory cells such as monocytes. Given its selective expression in crMPs, we
318 believe that targeting of *Schlafenlnc* warrants further exploration as a potential anti-inflammatory
319 therapeutic strategy.

320 Similar to its orthologue in mice, human *Schlafenlnc* is specific for immune cell types (Extended Data
321 Fig. S4A). In support of conserved function in immune cells, our protein interactor analysis of both
322 murine and human *Schlafenlnc* using deep learning showed similar binding modules for RNA binding
323 proteins (Extended Data Fig. S4B and S4C). Further studies will be required to dissect molecular
324 interactors for *Schlafenlnc* in mouse and human.

325 Taken together, our study demonstrates that lncRNAs act as critical contributors to the
326 transcriptome-based analysis of cell clusters in line with their crucial role in development and cell fate
327 determination[3], leading to the definition of cell identities. The combination of single cell sequencing and
328 RNA-Seq approaches led us to the identification of multiple novel candidate lncRNAs that warrant
329 further analysis in cardiac homeostasis and disease. One of the most abundant and macrophage-
330 enriched lncRNAs, *Schlafenlnc*, acts as a crucial regulator of macrophage adhesion and migration.

331 **METHODS**

332 Experimental animals, surgery conditions

333 Surgeries on mice were performed according to the guidelines and regulations of the responsible
334 authorities. Consent was given by the institutional review board of the Regierung of Oberbayern (ROB-
335 55.2-2532.Vet_02-19-194).
336 Wild type male mice of C57BL/6N background were purchased from Jackson Laboratories and
337 submitted to transverse aortic constriction (TAC) or sham procedure as reported previously[16] at an age
338 of 8-10 weeks.

339 To produce *Schlafenlnc* -knockout mice, two sgRNAs (5' cut site: 5'- GAGGTTCCATCAGTCTGACA-
340 3', 3' cut site: 5'-ACATGTCTTTGGTAGGAGCA-3') targeting the flanking region of the *Schlafenlnc* gene
341 in the mouse genome were designed and synthesized by IDT (Coralville, IA, USA). A mixture of Cas9
342 protein (IDT) and sgRNAs was electroporated into C57BL/6 mouse zygotes. Genomic DNA of newborn
343 mice was amplified using the primers Slfnlnc1 (5'-TTCCTTCAGAGGTCCATCAG-3') and Slfnlnc4 (5'-
344 AGCCAGTCTAAAGACTCTGG-3'). The appearance of a 360 bp band identified founder mice with a
345 complete loss of the *Schlafenlnc* gene. The animals were bred to homozygosity and used for the
346 experiments.

347 Echocardiography was performed as reported before[16].

348 Primary cell isolation from adult murine heart

349 Hearts of C57BL/6N mice were harvested at an age of 8-10 weeks and subjected to digestion by
350 perfusion via the coronary arteries using Collagenase II (Worthington, Lakewood, NJ) as described
351 previously[66]. Cell suspension was processed according to subsequent protocol/experiment.

352 Single cell cloning and sequencing

353 Primary cells from a sham[16] and an adult mouse heart 6d after TAC were washed three times with PBS
354 to remove cell debris and passed successively through 100µm, 70µm and 30µm filters. The single cell
355 library was generated using the Chromium Single Cell 3' GEM, Library & Gel Bead Kit v2 (10X
356 Genomics) with a target of 10,000 cells per sample. The single cell library was cloned according to the
357 manufacturer's instructions. Sequencing was performed on a HiSeq4000 (Illumina).

358 Primary cells from the hearts from *Schlafenlnc*$^{-/-}$and littermate wildtype mice in basal condition as well
359 as after 6d TAC were passed through a 100µm filter and centrifuged for 1min at 100*xg* to pellet
360 cardiomyocytes. The supernatant (non-myocytes) was passed through a 40µm filter and washed twice
361 in magnetic-activated cell sorting (MACS) buffer (PBS + 0.5% BSA + 2mM EDTA) to result in 200µl cell
362 suspension. For the isolation of PBMCs, blood was diluted with 5 ml of MACS buffer and layered onto
363 5ml of Ficoll-Paque (17144002, Cytiva), followed by centrifugation at 400xg and 4°C for 30min in a
364 swinging rotor without a brake. The white layer containing the cells was aspirated, transferred to a 50ml
365 tube and mixed with 30ml of MACS buffer. After centrifugation for 5 min at 300xg and 4°C, the pellet
366 was washed once more with 30ml MACS buffer (200xg and 4°C for 5min) and resuspended in 200µl

367 MACS buffer. Cardiac and blood leukocytes (basal condition) were further purified using MACS, labelled
368 with cell hashing antibodies and isolated by FACS (all steps at 4°C): Cell suspensions were incubated
369 with Fc-block (1:50, BD Pharmingen 553142) for 10min and subsequently incubated with mouse CD45
370 MicroBeads (Miltenyi Biotec) for 15min. Cells were washed with MACS buffer and MACS was performed
371 using an AutoMACS (Miltenyi Biotec) running the program *possel_s*. After elution, pelleted cells were
372 resuspended in MACS buffer containing anti-CD45-FITC (1:1000, clone 30-F11, Biolegend, 103108),
373 PI (1:100) and cell hashing antibodies (1:1000, #1 for heart, #2 for blood, Biolegend) and incubated for
374 30min protected from light. For TAC samples, PBMCs were purified as above, cardiac non-myocytes
375 were directly used for cell sorting. Both cell fractions were stained with cell hashing antibodies (1:1000,
376 #2 for heart, #3 for blood, Biolegend) and Propidium iodide (1:100, Thermo) and incubated for 30min.
377 After washing, live cells of all samples were sorted on a Sony cell sorter SH800S, heart and blood cells
378 of each genotype and condition were pooled and run on a Chromium controller using the Chromium
379 Next GEM Single Cell 3' v3.1 Library & Gel Bead Kit (10X Genomics) with a target of 10,000 cells per
380 pool. Libraries were cloned according to the 10x Genomics user guide with feature barcode technology
381 for cell surface protein (RevD) and Biolegend's protocol for amplification of the cell hashing libraries.
382 Libraries were pooled according to the recommendations of 10x genomics protocol and sequenced on
383 a NovaSeq6000 (Illumina).

384 Purification of primary cells and cardiac macrophages by F4/80 MACS and cell sorting for RNA-seq

385 For a total myocardial cell sample, 100µl of the raw cell suspension of primary cells from adult wildtype
386 mouse hearts were washed twice with PBS and lysed in Trizol (ThermoFisher) for subsequent RNA
387 preparation. For the purification of cardiac macrophages, the cell suspension was filtered through cell
388 sieves of 70µm and 40µm of size and centrifuged at 100 *x g* for 3min at 4°C to completely remove
389 cardiac myocytes. All following steps were performed on ice/at 4°C. The supernatant (non-myocytes)
390 was washed twice in magnetic-activated cell sorting (MACS) buffer (PBS + 0.5% biotin-free BSA + 2mM
391 EDTA). MACS was performed in a two-step process using anti-F4/80-biotin coupled antibody (clone
392 BM8, Biolegend, 123106) and Streptavidin microbeads (Miltenyi Biotec) on LS columns (Miltenyi
393 Biotec). The eluted macrophage fraction was resuspended in a final volume of 200µl MACS buffer and
394 incubated 10 min with Fc block (1:50, BD Pharmingen). 200µl of staining solution containing flow
395 cytometry antibodies (anti-CD45-PECy7 (1:100, clone 30-F11, Invitrogen, 25-0451-82), anti-CD64-
396 PE/Dazzle594 (1:50, clone X54-5/7.1, Biolegend, 139320), anti-CD11b-PE (1:100, clone M1/70, BD
397 Pharmingen, 557397)) was added and incubated for 30min in the dark. Cells were washed twice with
398 MACS buffer and sorted on a Biorad S3 cell sorter. CD45+/CD64+/CD11+ macrophages were collected
399 (between 100k-170K cells), washed with PBS and lysed in Trizol (Invitrogen) for RNA preparation.

400 Fibrosis staining

401 Paraffin sections (8 µm) of ventricular myocardium were stained with Sirius red and Fast green. Images
402 of the whole heart were taken with a 10x objective using a AxioObserver.Z1 (Zeiss) motorized scanning-
403 stage microscopy (130 x 85; Märzhäuser). Fibrosis of the left ventricular myocardium was quantified as
404 the ratio of signals from Sirius red to Fast green in each section using the Metamorph software
405 (Molecular Devices).

406 CD68 staining

407 Cryosections (5 µm) of ventricular myocardium were fixed with methanol for 10 min at -20°C, washed
408 thoroughly with tap water and treated with acetone for 1 min at -20°C. Sections were air dried and
409 subsequently blocked with 5% goat serum in PBS for 1 h. Sections were stained with anti-mouse CD68
410 (1:100, clone FA-11, AbD Serotec, MCA 1957) at 4°C overnight. The sections were washed three times
411 with PBS + 0.05 % Tween 20 and stained with anti-rat AF564 (1:100, Invitrogen, A11007) and SYTOX™
412 Green (1:1000, Life technologies, S7020). Images were acquired by confocal microscopy using 63x
413 glycerol objective (Leica SP5) and analyzed using Metamorph (Molecular Devices).

414 Generation of knockout macrophages

415 Conditionally immortalized hematopoietic progenitor cells were generated from a R26-Cas9-eGFP
416 transgenic mouse line[41] as previously described[40]. For inducing CRISPR-Cas9 mediated knockout in
417 Hoxb8-FL cells, cells were electroporated with an sgRNA pair targeting the *Schlafenlnc* locus (IDT: Alt-
418 R® CRISPR-Cas9 sgRNA, 5' cut site 5'-GAGGTTCCATCAGTCTGACA-3', 3' cut site 5'-
419 GGCTTGGAAGTAGAAAACCG-3'), as control, a single sgRNA was used (5'-
420 ACCCCTTCAGCTTCACCTCC-3'). Transfected cells were single-cell cloned by limiting dilution assay
421 into 96-well plates and screened for knockout clones. CRISPR-directed deletions on *Schlafenlnc* were
422 identified by a PCR-based strategy to amplify the genomic DNA of the clones. Single-cell clones carrying
423 the induced deletions were expanded and frozen for further use. To do this, extraction of genomic DNA
424 was performed with QuickExtract™ DNA Extraction Solution (Lucigen) according to the manufacturer's
425 instruction. Briefly, approximately 100,000 cells were lysed in 50µl of QuickExtract by incubation as
426 follows: 65°C – 15min, 68°C – 15min, 98°C – 10min. 50ng of genomic DNA was then subjected to PCR
427 amplification with two primer pairs to distinguish successful *Schlafenlnc* knockout clones from wildtype
428 or heterozygous knockout. *Schlafenlnc*_KO_forward 5'-CAGCCCTGAGTCAGAACATAC-3' and
429 *Schlafenlnc*_KO_reverse 5'-TCCTTAGGGTGCACATCTACT-3' were used for detection of a
430 successfully cut site with a resulting amplicon length of 480bp, *Schlafenlnc*_WT_forward 5'-
431 TCTGTCTCTACTCCCTCAACTC-3' and *Schlafenlnc*_WT_reverse 5'-AAGGCATGTTCTGCTCCTAC-
432 3' were used for detection of the wildtype allele/uncut gene locus with a resulting amplicon length of
433 320bp.

434 Hoxb8-FL *Schlafenlnc* KO cell culture and differentiation

435 Hoxb8 progenitor cells were cultured in RPMI 1640 supplemented with 10% FCS, 1% Pen/Strep, 50
436 ng/mL FLT3L, 50nM b-mercaptoethanol and 1nM b-estradiol. FLT3L supernatant was obtained from a
437 FLT3L-producing B16 melanoma cell line.
438 For differentiation of HoxB8 cells into macrophages, Hoxb8 progenitor cells were cultured in
439 differentiation medium consisting of the culturing medium described above without b-estradiol and
440 supplemented with 20% MCSF supernatant, which was obtained from a MCSF-producing L929 cell line.
441 Differentiation was accomplished after 6 days.

442 Generation of bone marrow-derived macrophages

443 Femurs and tibias from 6-12 week old C57BL/6N mice were prepared and bone marrow was isolated
444 by flushing the bones with R10 medium (RPMI medium, 10% FCS, 1% antibiotics) with a syringe. To
445 generate bone marrow derived macrophages, 3-4 mio. isolated bone marrow cells were seeded in a
446 10cm petri dish containing R10 medium supplemented with 20% MCSF supernatant. Medium was
447 added on day 3 and exchanged on day 6 after seeding, macrophages were fully differentiated on day 8
448 and used for experiments.

449 Cytoplasmic/nuclear fractionation

450 Cytoplasmic/nuclear fractionation was performed as described before[67]. Briefly, bone marrow-derived
451 macrophages (BMDMs) were washed two times with cold PBS and harvested. 10% of the cells was
452 transferred into a new tube and used as a sample for the total gene expression. Cells were centrifuged
453 at 200 *x g* for 10 minutes and the total expression sample was directly used for RNA isolation. The
454 fractionation sample was resuspended in 200µl lysis buffer A (10 mM Tris pH=8, 140 mM NaCl, 1.5 mM
455 MgCl2, 0.5% Nonidet P-40) and incubated for 5 minutes on ice. The lysate was centrifuged at 1000 *x g*
456 for 3 minutes at 4°C. The supernatant containing the cytoplasmic fraction was directly used for RNA
457 isolation through lysis with Trizol. The sediment containing the nuclear fraction was washed two times
458 with lysis buffer A and one time with lysis buffer B (Buffer A supplemented with 1% Tween-40, 0.5%
459 deoxycholic acid) and afterwards resuspended in Trizol for RNA isolation.

460 RNA cloning and sequencing

461 Libraries from primary cardiac macrophages and total myocardium as well as *Schlafenlnc*-deficient and
462 control cell lines were generated using the TruSeq Stranded RNA Kit (Illumina) according to the
463 manufacturer's protocol, except for one step. Instead of using the SuperScriptII (ThermoFisher) as the
464 reverse transcriptase, SuperScriptIII (ThermoFisher) was used at a reaction temperature of 50°C.
465 Sequencing was performed on a HiSeq4000 platform (Illumina).
466 Libraries from fractionation samples were generated using the Stranded mRNA Prep, Ligation Kit
467 (Illumina) according to the manufacturer's instructions. Sequencing was performed on a NovaSeq6000
468 machine (Illumina).

469 RNA *in situ* hybridization (RNAscope)

470 Bone marrow derived macrophages were seeded on a removable 8-well chambers slide (Ibidi) and RNA
471 *in situ* hybridization was performed using the RNAscope Fluorescent Multiplex Reagent Kit (Advanced
472 Cell Diagnostics (ACD)) according to manufacturer's instructions. A custom designed RNA probe by
473 ACD was used for detection of *Schlafenlnc* (ENSMUST00000143673.2). Following the RNA *in situ*
474 hybridization, the slides were incubated with Phalloidin-AF647 (Abcam) for 60 minutes at room
475 temperature. Subsequently, slides were washed three times with PBS and mounted using ProLong™
476 Gold Antifade Mountant (Invitrogen). Images were acquired using the confocal microscope Leica TCS
477 SP II and the Leica Application Suite.

478 Galectin-3 ELISA

479 Cell culture supernatant of differentiated Hoxb8 macrophages was collected and the amount of soluble
480 Galectin-3 was quantitatively assessed using the Galectin-3 Mouse SimpleStep enzyme-linked immuno-
481 sorbent assay (ELISA) kit (Abcam) according to the manufacturer's instructions. The cell culture
482 supernatant was diluted 1:10 in sample diluent before use.

483 Chemotaxis

484 An IncuCyte® ClearView 96-Well Chemotaxis Plate (Sartorius) was coated on both sides of the
485 membrane using 50 µg/mL Matrigel (Corning) at 37°C for 30 minutes. After coating, plates were
486 incubated at room temperature for 30 minutes and afterwards washed with D-PBS. Differentiated HoxB8
487 macrophages were harvested and 2,000 cells were seeded in each well in differentiation medium
488 containing 0.5% FCS. Cells were allowed to settle at the bottom of the upper well for 30 minutes.
489 Subsequently, 100nM recombinant murine C5a (Pepro Tech) was added to the lower well of the
490 ClearView migration plate. Cells were imaged every 2 h for 72 hours using an Incucyte ZOOM
491 instrument and a 10x objective with chemotaxis plate settings. Chemotaxis was analyzed using the
492 IncuCyte ZOOM software.

493 Adhesion Assay

494 Ibidi black 96 well µ-Plate was coated with 20µg/mL Fibronectin (Sigma Aldrich) for 1 h at 37°C. 10,000
495 differentiated Hoxb8 macrophages were seeded in each well in differentiation medium and were
496 incubated for 2 hours at 37°C in a 5% CO2 atmosphere. After the incubation, cells were stained using
497 NucBlue Live ReadyProbes reagent (Invitrogen) and following the manufacturers' instructions. Images
498 of the Nuclei were taken before and after removing the non-adherent cells by washing three times with
499 pre-warmed medium using an EVOS FL Auto 2 cell imaging system (Invitrogen). Cell nuclei were
500 counted automatically using the MetaMorph analysis software (Molecular Devices).

501 Northern blotting

502 Northern blotting was performed as reported previously[68]. Briefly, 10µg total RNA from fibroblasts
503 (NIH/3T3) and *in vitro* differentiated macrophages were run on a 1.2% formaldehyde agarose gel,
504 transferred to a Hybond-N+ membrane (Ge Healthcare) and UV-crosslinked. Probes were end-labelled
505 using [gamma-^{32}P]-ATP and purified using an Illustra ProbeQuant G-50 micro column (GE Healthcare).
506 A mixture of two different probes was used per target. Probes were incubated over night with a pre-
507 hybridized membrane, signal was accumulated using a phophoimager screen and detected using a
508 Cyclone Plus (PerkinElmer). mGAPDH probe1 5'-
509 CATGGACTGTGGTCATGAGCCCTTCCACAATGCCAAAGTTG-3', mGAPDH probe2 5'-
510 GAATTTGCCGTGAGTGGAGTCATACTGGAACATGTAGACCATGTAGTTGAGG-3', Slfnlnc probe1
511 5'-CAGCTCTGCGTCTCTGCTCCTGTTCAGGTCCATCTTTCATCTCCG-3', Slfnlnc probe2 5'-
512 CAGTCGGGGTTCTGCCTCTTGATGTGGTTGTGCTAACCGGTGGGAC-3'.

513 *In vitro* transcription of 3´-biotinylated *SchlafenInc* sense or antisense RNA probe

514 The *SchlafenInc* sense and antisense (control) sequence was amplified from a vector containing the full
515 *SchlafenInc* (*AI662270-202*) sequence using Phusion DNA polymerase and the primers stated below.
516 RNA probes for the RNA pulldown were *in vitro* transcribed from the amplified sequence using T7 RNA
517 polymerase for 2h at 37°C. The probes were purified using illustra™ MicroSpin™ G-50 columns (GE
518 Healthcare) and afterwards biotin labelled using the Pierce™ RNA 3' End Biotinylation Kit (Thermo
519 Scientific) and following the manufacturers' instructions. RNA was extracted using Trizol and the quality
520 and purity of the RNA probes was analyzed by Sanger Sequencing and Tapestation (Agilent).

521 T7_Slfnlnc_sense_fwd 5'- TAATACGACTCACTATAGGGAAAGTCGCCTGGGGCCTC -3',
522 T7_Slfnlnc_sense_rev 5'- AATGAGCAAGATCCAACAACTTT -3', T7_Slfnlnc_antisense_fwd 5'-
523 TAATACGACTCACTATAGGGAATGAGCAAGATCCAACAACTTT -3', T7_Slfnlnc_antisense_rev 5'-
524 AAAGTCGCCTGGGGCCTC -3'.

525 RNA probes were folded directly before use by incubating 150ng of biotinylated purified RNA in 75µl
526 folding buffer (20mM Tris/HCl (pH 7.5), 100mM KCl, 10mM $MgCl_2$ and Rnase inhibitor (New England
527 Biolabs)) at 90°C for 2 minutes followed by incubation on ice for 3 minutes and finally incubation at room
528 temperature for 25 minutes.

529 RNA pulldown and mass spectrometry

530 10 million differentiated bone marrow-derived macrophages (isolated from C57BL/6N mice) were lysed
531 in 500µl lysis buffer (50mM Tris HCl (pH8), 150mM NaCl, 0.5% (v/v) NP-40 with Protease (cOmplete,
532 Roche) and Rnase inhibitor) for 30 minutes on ice. The lysate was centrifuged for 30 minutes at
533 17.000x*g* and 4°C. After the centrifugation, the supernatant was transferred into a new tube and 400µl
534 dilution buffer (20mM Tris/HCl (pH 7.4), 150mM NaCl, 2mM EDTA (pH 8.00), 0.5% Triton X-100 with
535 Protease and Rnase inhibitor) was added. 20µl streptavidin beads (Dynabeads M-270 Strepavidin,
536 Invitrogen) were washed and resuspended in 100µl dilution buffer. The streptavidin beads were added
537 to the diluted lysate and incubated for 30 minutes at 4°C with rotation to preclear the supernatant. After
538 the incubation time, the beads were removed from the mixture and an input sample was taken. 150 ng
539 *in vitro* transcribed 3´-biotinylated *SchlafenInc* sense or antisense (control) RNA probe was added to
540 the sample and incubated overnight at 4°C with rotation. 80 µl streptavidin beads were washed three
541 times with fresh dilution buffer and resuspended in 100µl dilution buffer. The beads were added to the
542 sample and incubated for three hours at 4°C with rotation. After the incubation time, the sample was
543 washed three times with 500 µl dilution buffer for 10 min at 4°C with rotation. The sample was washed
544 one more time with 500 µl dilution buffer containing 200 mM NaCl for 10 min at 4°C with rotation. The
545 sample was washed two more times with MS-washing buffer (10mM Tris pH 7.4, 150mM NaCl) and
546 analyzed with mass spectrometry. Liquid chromatography / mass spectrometry (LC/MS) was performed
547 on Thermo Scientific™ Q Exactive Plus equipped with an ultra-high performance liquid chromatography
548 unit (Thermo Scientific Dionex Ultimate 3000) and a Nanospray Flex Ion-Source (Thermo Scientific).
549 For data analysis MaxQuant 1.6.17.0[76], Perseus 1.6.1.3[77] and Excel (Microsoft Office 2016) were used.
550 N-terminal acetylation (+42.01) and oxidation of methionine (+15.99) were selected as variable

551 modifications and carbamidomethylation (+57.02) on cysteines as a fixed modification. Intensity based
552 absolute quantification values (iBAQ) were recorded. The mouse reference proteome set (Uniprot, April
553 2021, 55470 entries) was used to identify peptides and proteins with a false discovery rate (FDR) less
554 than 1%. Reverse identifications and common contaminants were removed. Proteins were filtered to be
555 identified at least 4 times (n=6) in one experimental group. Missing values were replaced by background
556 values from normal distribution. Significant interacting proteins were determined by student´s t-Test.

557 PURA Immunoprecipitation

558 50µl Dynabeads Protein G beads (Invitrogen) were washed with PBS and incubated with 1ml anti-PURA
559 antibody supernatant (monoclonal rat IgG2-2a anti-PURA[48], clone: 12D11) or control antibody (rat
560 IgG2a, clone: eBR2a, Invitrogen) overnight at 4°C with rotation. After the incubation, the beads were
561 washed two times with PBS and transferred to a fresh Eppendorf tube. Differentiated BMDMs (7-8 mio.
562 cells per sample, isolated from C57BL/6N mice) were washed and resuspended in 2 ml lysis buffer
563 (25mM Tris HCl (pH 7.4), 150mM KCl, 0.5% NP-40, 1mM EDTA (pH 8.0), protease (cOmplete, Roche)
564 and Rnase inhibitor (NEB)). Cells were sonicated for 30 seconds (Bandelin electronic sonicator UW
565 3100, duty cycle 0.5, amplitude 30%, MS72 tip) and incubated for 30 minutes on ice. The lysate was
566 centrifuged for 30 minutes at 17.000xg at 4°C and the supernatant was transferred to a fresh Eppendorf
567 tube. An input sample was taken at this point. The lysate was added to the magnetic beads and
568 incubated for 4 hours at 4°C with rotation. After the incubation, the beads were washed three times with
569 washing buffer (50mM Tris/HCl (pH 7.4), 150mM KCl, 0.1% NP-40, protease and Rnase inhibitor). The
570 PURA pull-down was confirmed with SDS-PAGE and Western blot and the *SchlafenInc* RNA as well as
571 a positive (*Tpt1*) and negative control (*Rpl32*) were measured by qPCR analysis.

572 Quantitative real-time PCR

573 1 µg of total RNA was reverse transcribed with Protoscript II reverse transcriptase (NEB), both according
574 to the manufacturer's instructions using random hexamer primers. Quantitative real-time PCR (qPCR)
575 was carried out with primers listed below, using the FastStart universal SYBR Green master mix
576 (Roche). The sample volume of 12.5 µl contained 1x SYBR Green master mix, 5 pmol of each primer
577 and 10 ng of cDNA. PCR was performed using StepOnePlus Real-Time PCR systems (Applied
578 Biosystems).

579 Slfnlnc_qPCR fwd 5'- ATGACTGGTCCTGGTTTTCG -3',
580 Slfnlnc_qPCR fwd 5'- TCTGCCTCTTGATGTGGTTG -3',
581 mRPL32 fwd (housekeeping gene) 5'- ACATCGGTTATGGGAGCAAC -3',
582 mRPL32 rev (housekeeping gene) 5'- GGGATTGGTGACTCTGATGG -3',
583 Tpt1 fwd (positive control for PURA IP) 5'- AGTCACCGGTGTTGACATTG -3',
584 Tpt1 rev (positive control for PURA IP) 5'- GCTCTGCAGCTCCAGTCATA -3'.

585

586 Data analysis

587 *Single cell sequencing data analysis*

588 Raw reads generated by single cell RNA sequencing data from sham[16] and 6d after TAC (this study)
589 was aligned against the mouse genome (mm10, Gencode annotation vM22[18]) using CellRanger 5.0.0
590 (10x Genomics). Cell that were called by CellRanger were subsequently analyzed using the R package
591 Seurat v3.2[69]. After quality control (retaining cells with >500 or <3,600 detected genes, <10%
592 mitochondrial cell content), 7,913 cells of the sham condition and 13,803 of the TAC condition were
593 used for further downstream analysis. SCTransform[70] was used to normalize and scale the data as well
594 as remove unwanted variation (regressing out mitochondrial gene content and cell cycle score).
595 SCTransform was then applied to identify variable feature which were used to integrate both data sets
596 ("IntegrateData" function). By using the ElbowPlot function on Principal Component Analysis results, the
597 number of relevant components was determined (set to 40) and used for embedding and visualization
598 by Uniform Manifold Approximation and Projection (UMAP). Seurat's "FindAllMarkers" function was
599 used for determination of cell population marker genes.

600 For the comparison of clusterings with adjusted Rand index score, gene sets were defined as follows:
601 all genes = all genes listed in the vM22 annotation of Gencode; protein coding genes = all genes with
602 gene biotype "protein coding" in vM22; lncRNAs = all genes in vM22 lncRNA annotation of Gencode
603 (gene biotype "lncRNA"+"TEC"); "expressed" gene sets = same definitions as above with filter for
604 average expression >0 in at least one cell cluster; all variable genes = gene list generated by Seurat's
605 "SelectIntegrationFeatures", default is 3,000 genes; subset of variable genes based on gene lists
606 defined above. Next, clusterings with resolutions from 0.01 to 1.00 with 0.01 increments were iteratively
607 calculated ("FindClusters" function) and cluster ID per cell was saved in a data frame. The adjusted
608 Rand Index is a measure for the degree of similarity between two clusterings, for example. The R
609 package mclust[71] with inbuilt function "adjustedRandIndex" was used to compare all gene sets to the
610 respective complete gene set (e.g. the subset of expressed lncRNAs to all expressed genes).

611 For calculating de-regulated genes after TAC, first Adaptively thresholded Low-Rank Approximation
612 (ALRA)[72] was performed in order to impute drop out gene expression values followed by using Seurat's
613 "FindMarkers" function to compare each cell population before and after TAC. For the analysis of
614 scRNA-seq data of *Schlafenlnc*-deficient and wildtype animals, raw reads from basal and 6d after TAC
615 from WT and KO were aligned against the mouse genome (mm10, Gencode annotation vM25[18]) using
616 CellRanger 6.0.1 (10x Genomics) and analyzed using the R package Seurat v3.2[69]. Quality control was
617 applied to basal (>200 or <5,000 detected genes, <10% mitochondrial cell content) and TAC (>200 or
618 <4,000 detected genes, <10% mitochondrial cell content) samples. SCTransform and FindAllMarkers
619 was applied as above to normalize, scale, integrate data and identify marker genes for cell populations.
620 The integrated object was subset on all cell clusters expressing *Cd45* (Leukocytes). Deregulated genes
621 were calculated using Seurat's "FindMarkers" function to compare each cell population between
622 *Schlafenlnc*-deficient and wildtype cells. GO Term analysis of the deregulated genes was performed
623 using "DAVID 2021"[73].

624 *Cell-cell communication analysis*

625 A subset of cells of interest from blood and heart of *SchlafenInc*-decient and wildtype *Cd45*+ (*Lyve1*
626 macrophages, *MHCII*-high macrophages, *Isg* macrophages, intermediate macrophages, classical
627 monocytes and non-classical monocytes) was used for analysis of secreted signaling pathways within
628 the CellChat database. The *SchlafenInc*-deficient and wildtype objects were analyzed separately using
629 CellChat[74] and merged with "mergeCellChat". The differential number of interactions between the cell
630 clusters in *SchlafenInc*-deficient vs. wildtype was analyzed and displayed using the CellChat function
631 "netVisual_diffInteraction" and the differential signaling pathways were assessed using "rankNet".

632 *Estimating RNA velocity*

633 To calculate the RNA velocity of single cells, the abundance of the spliced and unspliced RNA was
634 quantified by running Velocyto CLI (v0.17.5) on CellRanger output BAM files and the corresponding
635 gene annotation (GENCODE vM22). The resulting loom files were incorporated into the Seurat objects
636 using SeuratWrapper R package (v0.3.0), and after integration and clustering, the objects were
637 converted to AnnData format (h5ad) to be compatible for downstream analysis with the Python package
638 scVelo (v0.2.5). Using scVelo, cell-to-cell transition probabilities were estimated and RNA-velocity was
639 projected as streamlines on the UMAP embedding.

640 *Identification of novel lncRNAs*

641 Most steps of this pipeline were performed using the Galaxy platform[75]. Reads were mapped using RNA
642 STAR aligner (Galaxy version 2.6.0b-2)[76] using a built-in index based on Gencode vM22 annotation and
643 otherwise default parameters. StringTie (Galaxy Version 1.3.3.2)[77] was used to predict novel transcripts
644 (strand information RF, reference file Gencode vM22, average read length 90). StringTie merge (Galaxy
645 version 1.3.6) with default parameters was used to merge all new annotations together, including
646 Gencode annotation vM22 as reference annotation. Novel genes were extracted by Bedtools Intersect
647 tool (Galaxy version v2.29.0)[78], intersecting the merged annotation with the Gencode vM22 annotation.
648 Transcripts were extracted with the "Extract features" tool (Galaxy 1.0.0) and analyzed for coding
649 potential with FEELnc (Galaxy version 0.1.1.1)[30]. FEELnc produces a gene transfer format (gtf)
650 annotation file containing only transcripts classified as long non-coding RNAs. "cat" command was used
651 to merge this lncRNA annotation to Gencode vM22 reference annotation file to create reference
652 annotation file with additional novel lncRNA genes. All RNA-Seq libraries were measured again against
653 this new transcriptome using StringTie's "count" option. For visualizing coding probability, the python
654 version of the Coding-Potential Assessment Tool (CPAT, v2.0.0)[79] was run on the fasta sequences of
655 the novel lncRNAs ($ cpat.py -g novel_lncRNAs_gffread.fasta -d Mouse_logitModel_CPAT.RData -x
656 Mouse_Hexamer_CPAT.tsv -o output_novel_lncRNAs.txt). GraphPad Prism 8 was used to calculate
657 the frequency distribution in percentages. For plotting transcript lengths, the length determined in the
658 CPAT output was used and again transformed to frequency distribution in Prism. For the categorization
659 of interactions between lncRNAs and other genes, the classifier output of FEELnc was used.
660 Interactions with the same gene were discarded, for known lncRNAs only genes expressed
661 predominantly in cardiac macrophages were considered ($\log_2$ fold change >1). To compute differential
662 gene expression analysis, DESeq2 package was used (Galaxy version 2.11.40.2)[80], outputting also a
663 normalized counts file. Normalized counts served as input for clustering and heatmap visualization by
664 ClustVis R package (v. 0.0.0.9)[81].

665 *RNA-Seq analysis of Hoxb8 SchlafenInc-deficient macrophages*

666 Fastq reads were mapped using RNA STAR aligner (Galaxy version 2.6.0b-2)[76] using a built-in index
667 based on Gencode vM22 annotation and otherwise default parameters. StringTie (Galaxy Version
668 1.3.3.2)[77] count option was used to quantify gene expression using Gencode vM22 as reference
669 annotation. DESeq2 was used to calculate differential gene expression (Galaxy version 2.11.40.2)[80].
670 The normalized counts file was used for heatmap visualization with ln(x) transformation of the top 20
671 down-regulated genes (ClustVis R package[81]).

672 *Neighboring genes analysis and Gene Ontology Analysis*

673 Up- or downregulated lncRNAs during pressure overload (p-value<0.05) in either macrophage,
674 fibroblast or endothelial cell populations were analyzed for neighboring genes using FEELnc (Galaxy
675 Version 0.2[30]) and filtered for antisense protein coding genes. Gene ontology analysis for these gene
676 sets for each cell population was performed using the web-based tool "DAVID 2021"[73]. Neighboring
677 genes of known and novel lncRNAs were also identified using FEELnc (Galaxy Version 0.2[30]).
678 Biological processes associated with the differentially regulated genes in *SchlafenInc*-deficient
679 macrophages (log2FC > 1 or < -1, FDR < 0.05) were determined using ClueGO application (v2.5.8)[82]
680 ran within Cytoscape (v3.8.2)[83] network analysis tool (p-value cutoff = 0.01, Min GO level = 4, Max GO
681 Level = 10, Number of Genes = 2, Min. Percentage = 4.0).

682 *Kipoi RBP-eclip analysis (Protein interactors analysis)*

683 Model training data: To access the binding probability of known RBPs on *SchlafenInc*, a pretrained deep
684 neural network (DNN)[34] on eCLIP-seq data[35] was downloaded from the Kipoi repository[84]. In order to
685 test the binding probability of the 101 proteins on *SchlafenInc*, a bed file containing the coordinates of
686 *SchlafenInc*'s 4 exons (ENSMUST00000143673.2 on Ensembl) was obtained. Then for each exon, we
687 took sliding windows of 101nt length resulting on a new bed6 file where each row is of 101nt length.
688 Kipoi builds on environments, making the sharing and loading of models easy. We started our analysis
689 by generating an environment with all the needed dependencies. Afterwards for each protein of interest,
690 we programmatically obtained the dataloader, load the fasta sequence for GRCm38.p6, load the
691 GENCODE annotation for mouse version vM22[18], and a bed file with the pre-extracted 101nt length
692 sliding windows and ran the predict function with default arguments (considering all the genomic
693 landmarks also for non-protein coding genes). Finally, for each protein of interest a csv file was
694 generated, containing the following info for each 101nt sequence considered: the chromosome, the
695 starting position, the end position, a sequence ID, a score as in the bed6 file, the strand and the binding
696 score [0 (no binding probability), 1 (high binding probability)] of the protein of interest on that window.

697 <u>Software list</u>

698 Leica Application Suite Advanced Fluorescence, version 2.7.9723
699 Invitrogen EVOS FL Auto 2 Software
700 CellRanger, version 5.0.0
701 Seurat, version 3.2
702 RNA STAR aligner, version 2.6.0b-2
703 StringTie and StringTie merge, version 1.3.3.2 and 1.3.6

704 Bedtools Intersect tool, version v2.29.0
705 “Extract features” tool, version 1.0.0
706 FEELnc, version 0.1.1.1 (Galaxy) and version 0.2
707 Coding-Potential Assessment Tool, CPAT, version 2.0.0
708 DESeq2, version 2.11.40.2
709 ClustVis R package, version 0.0.0.9
710 Cytoscape, version 3.8.2
711 ClueGO, version 2.5.8
712 MetaMorph Offline, version 7.10.1
713 Prism 8 for Mac OS, version 8.4.1
714 Adobe Illustrator for Mac OS, version 24.2.1
715 R studio, version 3.6.3
716 Microsoft Office for Mac

717 Statistical Analysis

718 Statistical analysis was performed using GraphPad Prism 8. To test for outliers Grubbs test (alpha=0.05)
719 was used. Data distribution and the difference between variances were tested using the Shapiro-Wilk
720 normality test. For statistical analysis of two groups, unpaired t-test was performed for normal distributed
721 samples, otherwise Mann-Whitney test was used. For more than two groups, two-way ANOVA was
722 performed. For chemotaxis experiments, area under the curve (AUC) was calculated and statistical
723 significance was tested using unpaired t-test. Significance is depicted as *$p < 0.05$, **$p < 0.01$,
724 ***$p < 0.001$, ****$p < 0.0001$.

ACKNOWLEDGEMENT

We thank Lucia Koblitz for expert support with primary cell preparations, Julia Kerler and Anton Bomhard for expert assistance in animal surgeries and Dr. Elisabeth Graf for assistance with RNA-seq. We thank Dr. Daniel Andergassen and Dr. Bernhard Laggerbauer for critical reading and helpful discussions.

FUNDING

This project was funded by the Deutsche Forschungsgemeinschaft (DFG, German Research Foundation)—Project- ID 403584255–TRR 267 (S.E., A.D., R.P.B., M.S.L., L.M., T.M., J.G., I.W.). S.E., A.D., L.A., D.E., K.H., N.P., H.S., C.S., T.W., J.G., E.T., H.B.S., T.M., N.J., M.S.L. and R.P.B. were supported in the framework of the German Centre for Cardiovascular Research (DZHK), and the partner site in Munich (MHA) (S.E., A.D., H.S., C.S., T.W., J.G., H.B.S., T.M.) projects 81X3600404 (A.D.), 81X2600245 (C.S.) and 81X2600246 (C.S.) or partner site RheinMain, Frankfurt (N.J., M.S.L. and R.P.B.). S.E. and D.R. were supported by DFG through the Research Training Group GRK2338 and the European Union's Horizon 2020 research and innovation programme under the Marie Skłodowska-Curie grant agreement no. 813716.

Author contributions

A.D. and S.E. designed the study and wrote the manuscript. A.D., L.A. D.E., S.B., E.T., K.H., N.P., A.U. and I.W. performed the experiments or analyzed the resulting data. M.B. provided the *Schlafenlnc* knockout mouse. R.P.B., J.G., P.K., M.S.L., L.M., T.M., D.R., H.B.S., M.S.-S., C.S., D.N. and T.W. provided experimental models, instruments and crucial expertise.

CONFLICT OF INTEREST

None declared.

746 **REFERENCES**

747 1. Goodall, G. J. & Wickramasinghe, V. O. RNA in cancer. *Nat. Rev. Cancer* **21**, 22–36 (2021).
748 2. Aliperti, V., Skonieczna, J. & Cerase, A. Long non-coding rna (Lncrna) roles in cell biology,
749 neurodevelopment and neurological disorders. *Non-coding RNA* **7**, (2021).
750 3. Anderson, K. M. & Anderson, D. M. LncRNAs at the heart of development and disease.
751 *Mamm. Genome* **33**, 354–365 (2022).
752 4. Wysoczynski, M., Kim, J., Moore, J. B. & Uchida, S. Macrophage long non-coding rnas in
753 pathogenesis of cardiovascular disease. *Non-coding RNA* **6**, 1–18 (2020).
754 5. Klattenhoff, C. A. *et al.* Braveheart, a long noncoding RNA required for cardiovascular lineage
755 commitment. *Cell* **152**, 570–583 (2013).
756 6. Li, K. *et al.* A noncoding antisense RNA in tie-1 locus regulates tie-1 function in vivo. *Blood*
757 **115**, 133–139 (2010).
758 7. Micheletti, R. *et al.* The long noncoding RNA Wisper controls cardiac fibrosis and remodeling.
759 *Sci. Transl. Med.* **9**, (2017).
760 8. Zaman, R. & Epelman, S. Resident cardiac macrophages: Heterogeneity and function in health
761 and disease. *Immunity* **55**, 1549–1563 (2022).
762 9. Gomez Perdiguero, E. *et al.* Tissue-resident macrophages originate from yolk-sac-derived
763 erythro-myeloid progenitors. *Nature* **518**, 547–551 (2015).
764 10. Epelman, S. *et al.* Embryonic and adult-derived resident cardiac macrophages are maintained
765 through distinct mechanisms at steady state and during inflammation. *Immunity* **40**, 91–104
766 (2014).
767 11. Dick, S. A. *et al.* Three tissue resident macrophage subsets coexist across organs with
768 conserved origins and life cycles. *Sci. Immunol.* **7**, 1–19 (2022).
769 12. Hulsmans, M. *et al.* Macrophages Facilitate Electrical Conduction in the Heart. *Cell* **169**, 510-
770 522.e20 (2017).
771 13. Grune, J. *et al.* Neutrophils incite and macrophages avert electrical storm after myocardial
772 infarction. *Nat. Cardiovasc. Res.* **1**, 649–664 (2022).
773 14. Fujiu, K. *et al.* A heart-brain-kidney network controls adaptation to cardiac stress through tissue
774 macrophage activation. *Nat. Med.* **23**, 611–622 (2017).
775 15. Cahill, T. J. *et al.* Tissue-resident macrophages regulate lymphatic vessel growth and
776 patterning in the developing heart. *Dev.* **148**, (2021).
777 16. Ramanujam, D. *et al.* MicroRNA-21–Dependent Macrophage-to-Fibroblast Signaling
778 Determines the Cardiac Response to Pressure Overload. *Circulation* **143**, 1513–1525 (2021).
779 17. Butler, A., Hoffman, P., Smibert, P., Papalexi, E. & Satija, R. Integrating single-cell
780 transcriptomic data across different conditions, technologies, and species. *Nat. Biotechnol.* **36**,
781 411–420 (2018).
782 18. Harrow, J. *et al.* GENCODE: The reference human genome annotation for the ENCODE
783 project. *Genome Res.* **22**, 1760–1774 (2012).
784 19. Skelly, D. A. *et al.* Single-Cell Transcriptional Profiling Reveals Cellular Diversity and
785 Intercommunication in the Mouse Heart. *Cell Rep.* **22**, 600–610 (2018).
786 20. McLellan, M. A. *et al.* High-Resolution Transcriptomic Profiling of the Heart during Chronic
787 Stress Reveals Cellular Drivers of Cardiac Fibrosis and Hypertrophy. *Circulation* 1448–1463
788 (2020) doi:10.1161/CIRCULATIONAHA.119.045115.
789 21. Mercer, T. R., Dinger, M. E., Sunkin, S. M., Mehler, M. F. & Mattick, J. S. Specific expression
790 of long noncoding RNAs in the mouse brain. *Proc. Natl. Acad. Sci. U. S. A.* **105**, 716–721
791 (2008).
792 22. Derrien, T. *et al.* The GENCODE v7 catalog of human long noncoding RNAs: Analysis of their
793 gene structure, evolution, and expression. *Genome Res.* **22**, 1775–1789 (2012).
794 23. Cabili, M. *et al.* Integrative annotation of human large intergenic noncoding RNAs reveals
795 global properties and specific subclasses. *Genes Dev.* **25**, 1915–1927 (2011).
796 24. Ulitsky, I. Evolution to the rescue: Using comparative genomics to understand long non-coding
797 RNAs. *Nat. Rev. Genet.* **17**, 601–614 (2016).
798 25. Piccoli, M.-T. *et al.* Inhibition of the Cardiac Fibroblast-Enriched lncRNA Meg3 Prevents
799 Cardiac Fibrosis and Diastolic Dysfunction. *Circ. Res.* CIRCRESAHA.117.310624 (2017)
800 doi:10.1161/CIRCRESAHA.117.310624.
801 26. Hofmann, P. *et al.* Long non-coding RNA H19 regulates endothelial cell aging via inhibition of
802 STAT3 signalling. *Cardiovasc. Res.* **115**, 230–242 (2019).
803 27. Han, P. *et al.* A long noncoding RNA protects the heart from pathological hypertrophy. *Nature*
804 **514**, 102–106 (2014).
805 28. Alexanian, M. & Haldar, S. M. The cardiac myofibroblast from supporting cast to leading role?

806 *Circ. Res.* **123**, 1258–1260 (2018).
807 29. Guttman, M. *et al.* Chromatin signature reveals over a thousand highly conserved large non-
808 coding RNAs in mammals. *Nature* **458**, 223–227 (2009).
809 30. Wucher, V. *et al.* FEELnc: A tool for long non-coding RNA annotation and its application to the
810 dog transcriptome. *Nucleic Acids Res.* **45**, 1–12 (2017).
811 31. Liu, F., Zhou, P., Wang, Q., Zhang, M. & Li, D. The Schlafen family: complex roles in different
812 cell types and virus replication. *Cell Biol. Int.* **42**, 2–8 (2018).
813 32. Hezroni, H. *et al.* Principles of Long Noncoding RNA Evolution Derived from Direct Comparison
814 of Transcriptomes in 17 Species. *Cell Rep.* **11**, 1110–1122 (2015).
815 33. Luo, Y. *et al.* New developments on the Encyclopedia of DNA Elements (ENCODE) data
816 portal. *Nucleic Acids Res.* **48**, D882–D889 (2020).
817 34. Avsec, Z., Barekatain, M., Cheng, J. & Gagneur, J. Modeling positional effects of regulatory
818 sequences with spline transformations increases prediction accuracy of deep neural networks.
819 *Bioinformatics* **34**, 1261–1269 (2018).
820 35. Van Nostrand, E. L. *et al.* Robust transcriptome-wide discovery of RNA-binding protein binding
821 sites with enhanced CLIP (eCLIP). *Nat. Methods* **13**, 508–514 (2016).
822 36. Dunham, I. *et al.* An integrated encyclopedia of DNA elements in the human genome. *Nature*
823 **489**, 57–74 (2012).
824 37. Shi, L., Shi, L., Wang, X. & He, J. Regulatory Roles of Osteopontin in Production of Monocyte-
825 Origin MCP-1. *Cell Transplant.* **27**, 1185–1194 (2018).
826 38. Gregory, J. L. *et al.* Macrophage Migration Inhibitory Factor Induces Macrophage Recruitment
827 via CC Chemokine Ligand 2. *J. Immunol.* **177**, 8072–8079 (2006).
828 39. Uhlén, M. *et al.* The human secretome. *Sci. Signal.* **12**, 1–9 (2019).
829 40. Redecke, V. *et al.* Hematopoietic progenitor cell lines with myeloid and lymphoid potential. *Nat.*
830 *Methods* **10**, 795–803 (2013).
831 41. Platt, R. J. *et al.* CRISPR-Cas9 knockin mice for genome editing and cancer modeling. *Cell*
832 **159**, 440–455 (2014).
833 42. Molitor, L., Bacher, S., Burczyk, S. & Niessing, D. The Molecular Function of PURA and Its
834 Implications in Neurological Diseases. *Front. Genet.* **12**, (2021).
835 43. Kanai, Y., Dohmae, N. & Hirokawa, N. Kinesin Transports RNA. *Neuron* **43**, 513–525 (2004).
836 44. Molitor, L. *et al.* Depletion of the RNA-binding protein PURA triggers changes in
837 posttranscriptional gene regulation and loss of P-bodies. *Nucleic Acids Res.* **51**, 1297–1316
838 (2023).
839 45. West, J. A. *et al.* The Long Noncoding RNAs NEAT1 and MALAT1 Bind Active Chromatin
840 Sites. *Mol. Cell* **55**, 791–802 (2014).
841 46. Marx, V. Method of the Year: spatially resolved transcriptomics. *Nat. Methods* **18**, 9–14 (2021).
842 47. Svensson, V. *et al.* Power analysis of single-cell rnA-sequencing experiments. *Nat. Methods*
843 **14**, 381–387 (2017).
844 48. Rhee, A. J. & Lavine, K. J. New Approaches to Target Inflammation in Heart Failure:
845 Harnessing Insights from Studies of Immune Cell Diversity. *Annu. Rev. Physiol.* **82**, 1–20
846 (2020).
847 49. Duncan, S. E. *et al.* Macrophage Activities in Myocardial Infarction and Heart Failure. *Cardiol.*
848 *Res. Pract.* **2020**, (2020).
849 50. Moskalik, A., Niderla-Bielińska, J. & Ratajska, A. Multiple roles of cardiac macrophages in
850 heart homeostasis and failure. *Heart Fail. Rev.* (2021) doi:10.1007/s10741-021-10156-z.
851 51. Peet, C., Ivetic, A., Bromage, D. I. & Shah, A. M. Cardiac monocytes and macrophages after
852 myocardial infarction. *Cardiovasc. Res.* **116**, 1101–1112 (2020).
853 52. Liao, X. *et al.* Distinct roles of resident and nonresident macrophages in nonischemic
854 cardiomyopathy. *Proc. Natl. Acad. Sci. U. S. A.* **115**, E4661–E4669 (2018).
855 53. Leuschner, F. *et al.* Rapid monocyte kinetics in acute myocardial infarction are sustained by
856 extramedullary monocytopoiesis. *J. Exp. Med.* **209**, 123–137 (2012).
857 54. Dutta, P. *et al.* Myocardial infarction activates CCR2+ hematopoietic stem and progenitor cells.
858 *Cell Stem Cell* **16**, 477–487 (2015).
859 55. Dutta, P. *et al.* Myocardial infarction accelerates atherosclerosis. *Nature* **487**, 325–329 (2012).
860 56. Aoki, S. *et al.* Elevated peripheral blood mononuclear cell count is an independent predictor of
861 left ventricular remodeling in patients with acute myocardial infarction. *J. Cardiol.* **57**, 202–207
862 (2011).
863 57. Van Der Laan, A. M. *et al.* A proinflammatory monocyte response is associated with
864 myocardial injury and impaired functional outcome in patients with ST-segment elevation
865 myocardial infarction: Monocytes and myocardial infarction. *Am. Heart J.* **163**, 57-65.e2 (2012).
866 58. Swirski, F. K. & Al., E. Identification of Splenic Reservoir. *Science (80-.).* **325**, 612–616 (2009).
867 59. Frantz, S. & Nahrendorf, M. Cardiac macrophages and their role in ischaemic heart disease.

Cardiovasc. Res. **102**, 240–248 (2014).
60. Bajpai, G. *et al.* Tissue Resident CCR2- and CCR2+ Cardiac Macrophages Differentially Orchestrate Monocyte Recruitment and Fate Specification Following Myocardial Injury. *Circ. Res.* **124**, 263–278 (2019).
61. Yakar Tülüce, S. *et al.* Galectin-3 levels in patients with hypertrophic cardiomyopathy and its relationship with left ventricular mass index and function. *Anatol. J. Cardiol.* **16**, 344–348 (2016).
62. Frunza, O. *et al.* Myocardial Galectin-3 Expression Is Associated with Remodeling of the Pressure-Overloaded Heart and May Delay the Hypertrophic Response without Affecting Survival, Dysfunction, and Cardiac Fibrosis. *Am. J. Pathol.* **186**, 1114–1127 (2016).
63. Danella Polli, C. *et al.* Monocyte Migration Driven by Galectin-3 Occurs through Distinct Mechanisms Involving Selective Interactions with the Extracellular Matrix. *ISRN Inflamm.* **2013**, 1–9 (2013).
64. Jia, W., Kidoya, H., Yamakawa, D., Naito, H. & Takakura, N. Galectin-3 accelerates M2 macrophage infiltration and angiogenesis in tumors. *Am. J. Pathol.* **182**, 1821–1831 (2013).
65. Papaspyridonos, M. *et al.* Galectin-3 is an amplifier of inflammation in atherosclerotic plaque progression through macrophage activation and monocyte chemoattraction. *Arterioscler. Thromb. Vasc. Biol.* **28**, 433–440 (2008).
66. Ramanujam, D., Sassi, Y., Laggerbauer, B. & Engelhardt, S. Viral vector-based targeting of miR-21 in cardiac nonmyocyte cells reduces pathologic remodeling of the heart. *Mol. Ther.* **24**, 1939–1948 (2016).
67. Hwang, H. W., Wentzel, E. A. & Mendell, J. T. A hexanucleotide element directs microRNA nuclear import. *Science (80-.).* **315**, 97–100 (2007).
68. Ziegler, C. *et al.* The long non-coding RNA LINC 00941 and SPRR 5 are novel regulators of human epidermal homeostasis . *EMBO Rep.* **20**, 1–13 (2019).
69. Stuart, T. *et al.* Comprehensive Integration of Single-Cell Data. *Cell* **177**, 1888-1902.e21 (2019).
70. Hafemeister, C. & Satija, R. Normalization and variance stabilization of single-cell RNA-seq data using regularized negative binomial regression. *Genome Biol.* **20**, 1–15 (2019).
71. Scrucca, L., Fop, M., Murphy, T. B. & Raftery, A. E. Mclust 5: Clustering, classification and density estimation using Gaussian finite mixture models. *R J.* **8**, 289–317 (2016).
72. Linderman, G. C., Zhao, J. & Kluger, Y. Zero-preserving imputation of scRNA-seq data using low-rank approximation. *bioRxiv* 397588 (2018) doi:10.1101/397588.
73. Sherman, B. T. *et al.* DAVID: a web server for functional enrichment analysis and functional annotation of gene lists (2021 update). *Nucleic Acids Res.* 1–6 (2022) doi:10.1093/nar/gkac194.
74. Jin, S. *et al.* Inference and analysis of cell-cell communication using CellChat. *Nat. Commun.* **12**, 1–20 (2021).
75. Afgan, E. *et al.* The Galaxy platform for accessible, reproducible and collaborative biomedical analyses: 2018 update. *Nucleic Acids Res.* **46**, W537–W544 (2018).
76. Dobin, A. *et al.* STAR: Ultrafast universal RNA-seq aligner. *Bioinformatics* **29**, 15–21 (2013).
77. Pertea, M. *et al.* StringTie enables improved reconstruction of a transcriptome from RNA-seq reads. *Nat. Biotechnol.* **33**, 290–295 (2015).
78. Quinlan, A. R. & Hall, I. M. BEDTools: A flexible suite of utilities for comparing genomic features. *Bioinformatics* **26**, 841–842 (2010).
79. Wang, L. *et al.* CPAT: Coding-potential assessment tool using an alignment-free logistic regression model. *Nucleic Acids Res.* **41**, 1–7 (2013).
80. Love, M. I., Huber, W. & Anders, S. Moderated estimation of fold change and dispersion for RNA-seq data with DESeq2. *Genome Biol.* **15**, 1–21 (2014).
81. Metsalu, T. & Vilo, J. ClustVis: A web tool for visualizing clustering of multivariate data using Principal Component Analysis and heatmap. *Nucleic Acids Res.* **43**, W566–W570 (2015).
82. Bindea, G. *et al.* ClueGO: A Cytoscape plug-in to decipher functionally grouped gene ontology and pathway annotation networks. *Bioinformatics* **25**, 1091–1093 (2009).
83. Shannon, P. *et al.* Cytoscape: A software Environment for integrated models of biomolecular interaction networks. *Genome Res.* **13**, 2498–2504 (2003).
84. Avsec, Ž. *et al.* The Kipoi repository accelerates community exchange and reuse of predictive models for genomics. *Nat. Biotechnol.* **37**, 592–600 (2019).

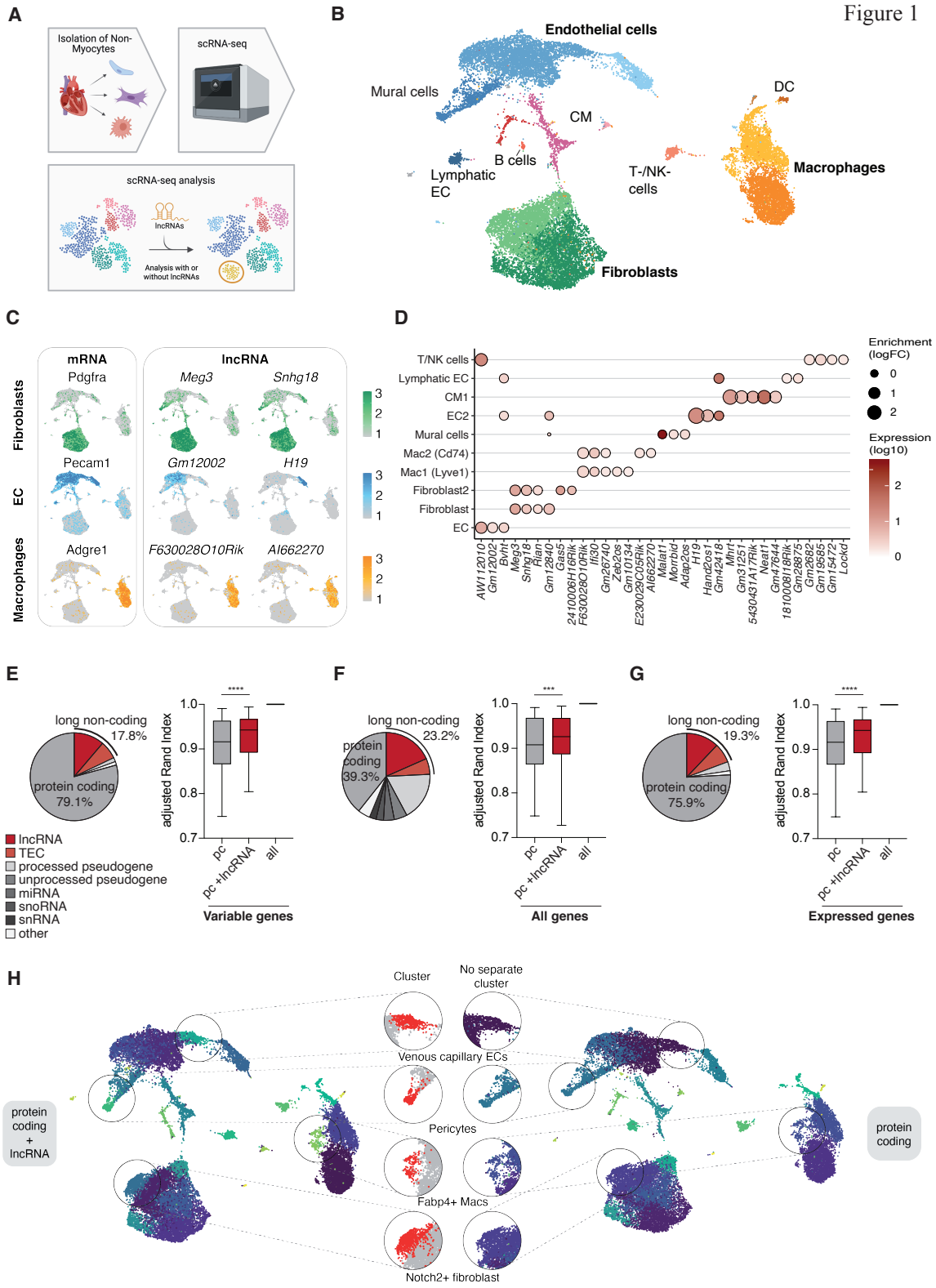

Figure 1: LncRNA are important determinants for definition of specific cell types.

(A) Illustration for the measurement of lncRNA in murine myocardium and re-clustering analysis. (B) UMAP projection of murine myocardium as measured by single-cell sequencing (scRNA-seq). Cell populations are colored by type as indicated by the label. DC: dendritic cells, EC: endothelial cells, CM:

931 cardiac myocytes. (C) Bubble plot showing lncRNA marker genes conserved across conditions. Bubble
932 size corresponds to enrichment (logFC) and fill color to expression value (log10). Only values/bubbles
933 with a significant enrichment (p-val < 0.05) are shown. (D) Feature plots showing mRNA and lncRNA
934 markers for fibroblasts, endothelial cells (EC) and macrophages. (E), (F), (G) Adjusted Rand Index (ARI)
935 calculation. In order to compare the clusterings with and without lncRNAs, the respective complete gene
936 set was considered to yield the optimal clustering. We iterated the clustering in 0.01 steps with
937 resolutions ranging from 0.10 to 1.00, testing for the similarity to optimal clustering using adjusted Rand
938 index scoring. Here, the more similar a clustering would be to the "optimal" one the closer it will be to 1.
939 Displayed as boxplot with median and quartiles. (E) ARI calculation for the top variable genes (3,000
940 genes). (F) ARI calculation for all annotated genes (Gencode vM22[18]). (G) ARI calculation for all
941 expressed genes (expression value >0). pc: protein coding (H) Umap projection of murine myocardium
942 with cell population clustering based on protein coding genes plus lncRNA genes (left panel) or only
943 protein coding genes (right panel). The middle panel shows differentially assigned cell population
944 clusters.

Figure 2

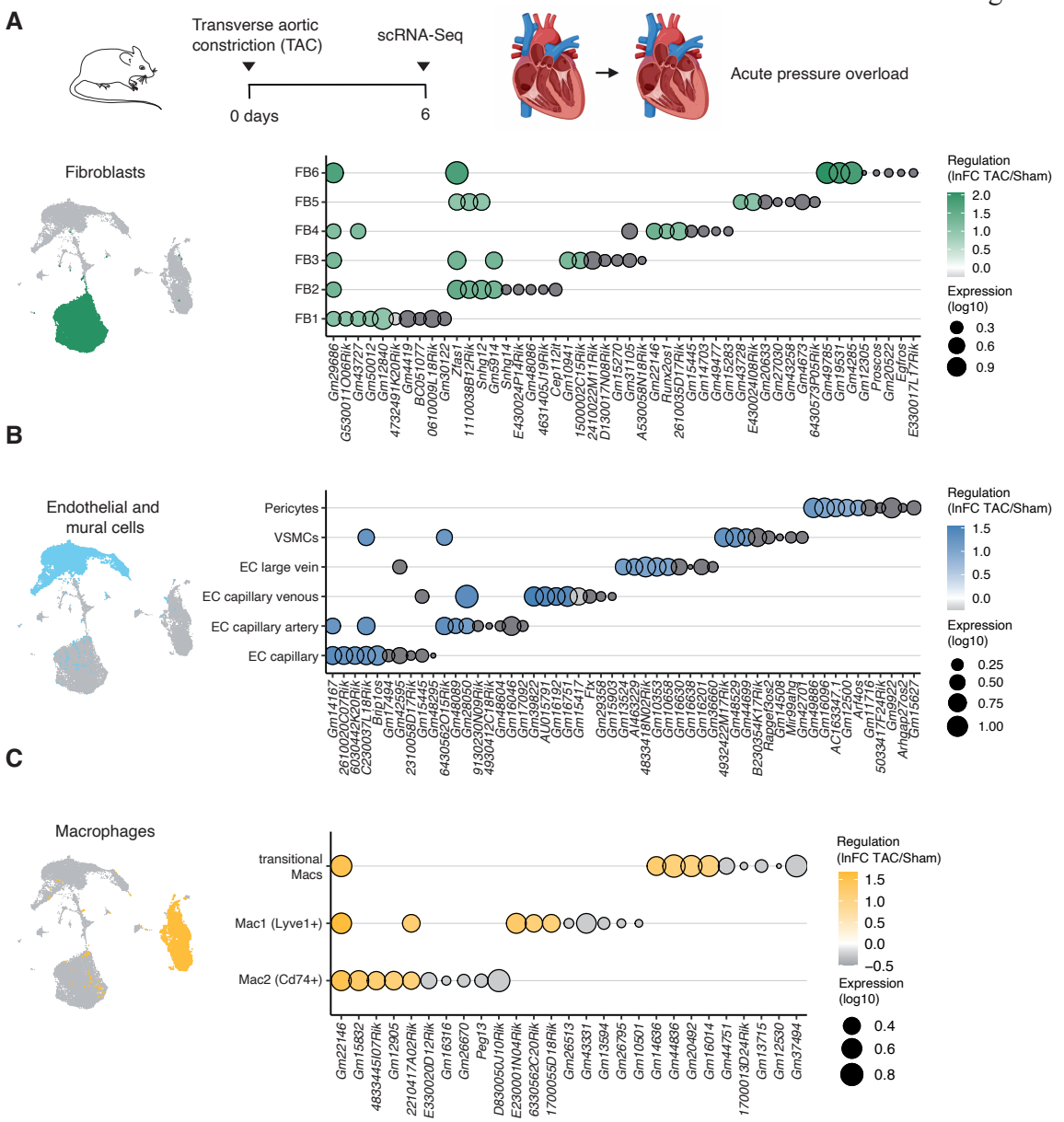

Figure 2: Dynamic changes of lncRNA expression in crMPs during pressure overload.

Bubble plot showing the top 5 up-regulated and top 5 down-regulated lncRNA genes after TAC for the sub-populations of the major cell types in the heart: (A) Fibroblasts (B) Endothelial cells and (C) Macrophages. Fill color corresponds to regulation in TAC vs. sham (lnFC TAC/sham) and bubble size corresponds to expression value (log10). Only values with a significant enrichment (p-val < 0.05) are shown. Some genes are among the top regulated genes in more than one cell type.

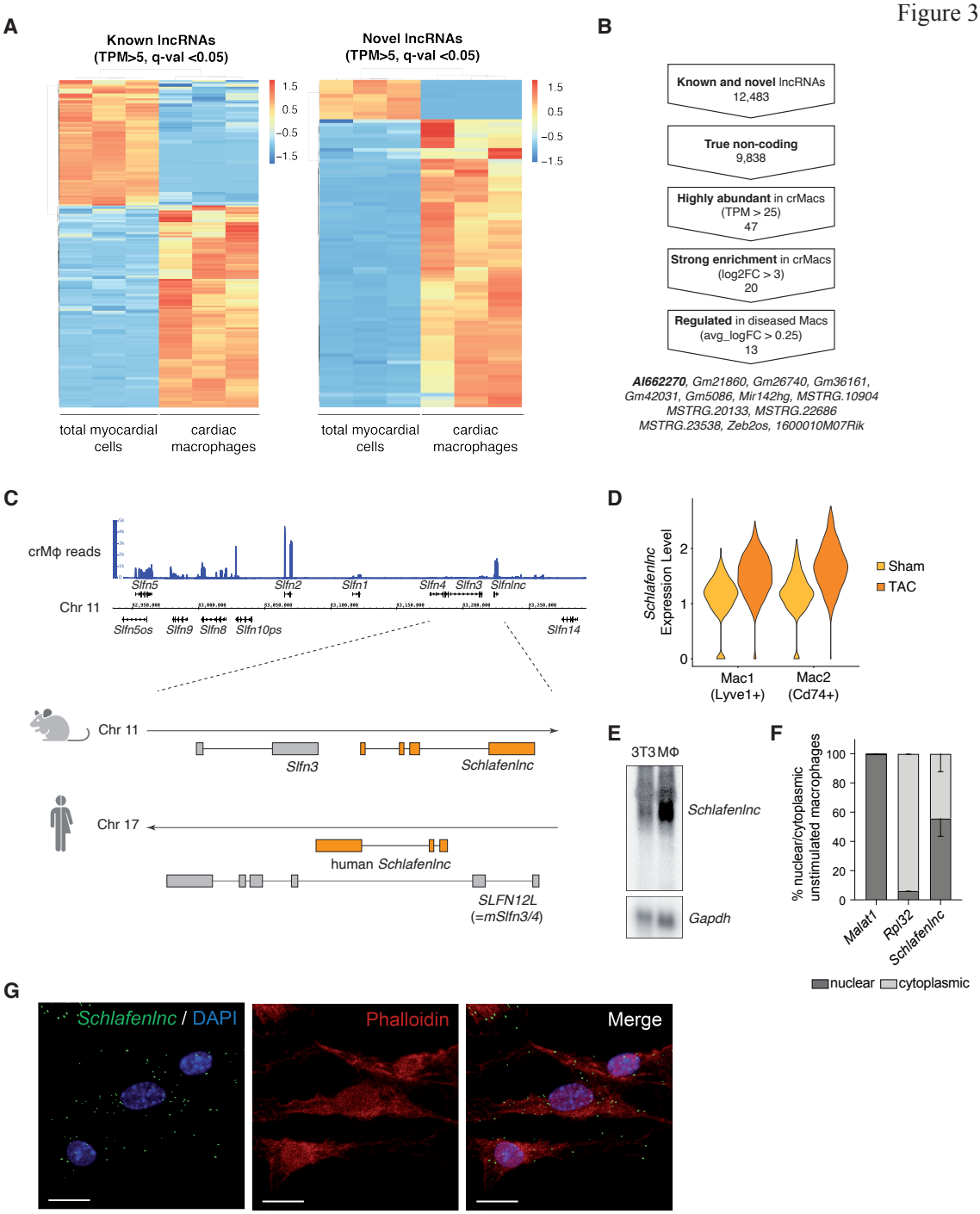

Figure 3: Determination and annotation of the lncRNA landscape of cardiac resident macrophages.

(A) Unsupervised clustering of known and novel lncRNAs using normalized counts values, rows were averaged across samples for clustering. Genes shown are expressed with a TPM value >5 and differentially regulated (enriched) with a q-val of <0.05. (B) Flow scheme for the identification of lncRNA candidates using the indicated filters. (C) The Schlafen family locus showing the expression in cardiac resident macrophages (accumulated plus and minus strand). Lower panel: Zoom in of the *Schlafenlnc* locus in mouse as well as human for comparison. (D) Expression of the lncRNA *Schlafenlnc* in Mac1 (*Lyve1*+ macrophages) and Mac2 (*MHCII* high, *Cd74*+ macrophages) after sham or TAC in the scRNA-

962 seq data. (E) Northern Blot showing the expression of *SchlafenInc* transcripts in bone marrow-derived
963 macrophages in comparison to fibroblasts (NIH3T3 cell line). (F) Relative nuclear and cytoplasmic
964 localization of *Malat1* (nuclear lncRNA), *Rpl32* (mRNA) and *SchlafenInc* as determined by fractionation
965 of macrophages followed by quantification through RNA-Seq. Data are normalized counts displayed as
966 mean with SEM. (G) Detection of *SchlafenInc* (green) in macrophages by RNA *in situ* hybridization
967 (RNAScope). Nuclei were stained with DAPI (blue), Phalloidin (red) was used for outlining the cellular
968 body (Scale bars = 15μm).

969

Figure 4

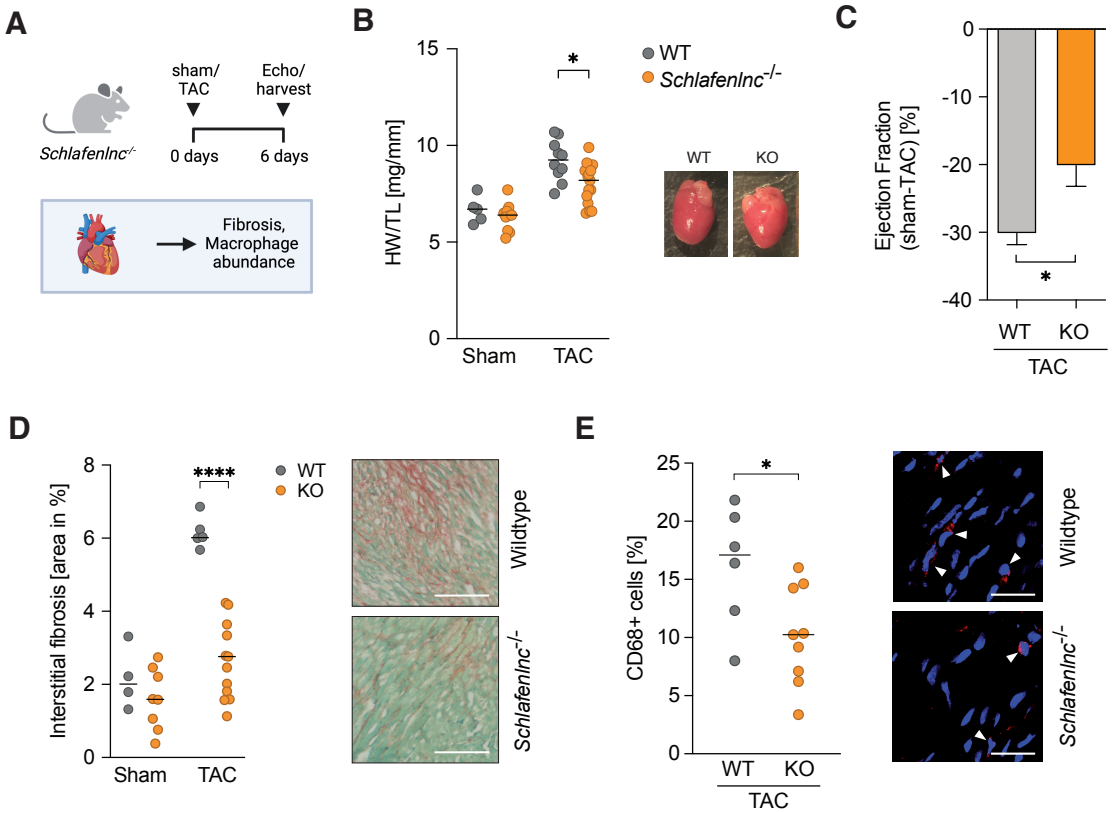

Figure 4: *SchlafenInc*-deficient mice show improved cardiac function and reduced inflammatory response after transverse aortic constriction (TAC).

(A) Experimental setup of cardiac phenotyping of *SchlafenInc*$^{-/-}$ and wildtype mice. (B) Quantification of normalized heart weight after TAC. HW= heart weight, TL= tibia length. Black line = median. C) Ejection fraction changes after 6 days TAC. Data displayed as mean with SEM. (C) Left: Quantification of interstitial fibrosis by Sirius red/Fast green staining. Black line = median. Right: Representative images of interstitial fibrosis, scale bar = 200µm. (D) Representative images and quantification of macrophage/monocyte content by CD68 staining in WT and *SchlafenInc*$^{-/-}$ hearts after 6d after TAC. Black line = median. White arrows label CD68-positive cells, scale bar = 25µm.

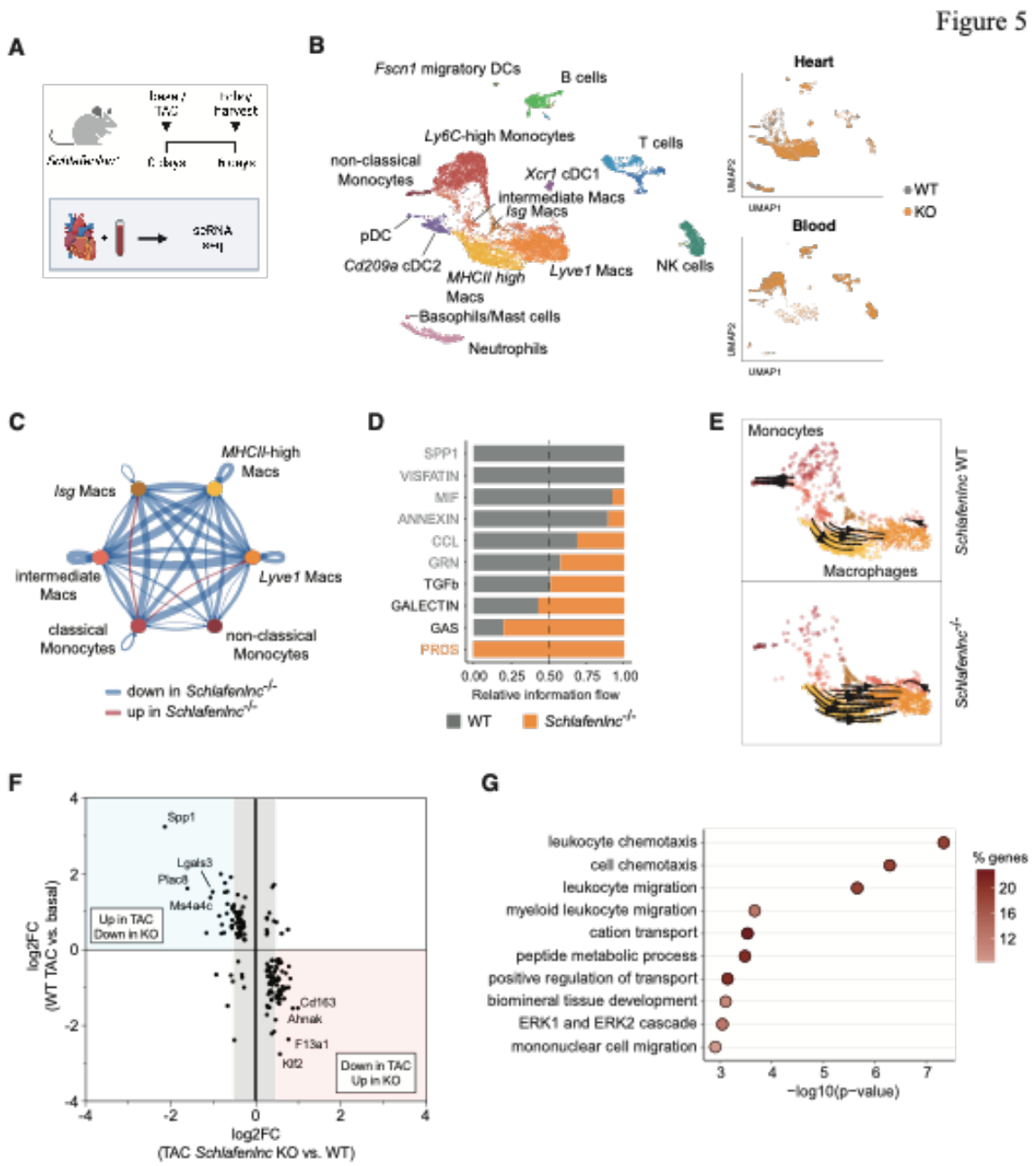

Figure 5: scRNA-seq of *Schlafenlnc*$^{-/-}$ mice reveals macrophage polarization towards an anti-inflammatory phenotype after TAC.

(A) Experimental setup of scRNA-seq of *Schlafenlnc*$^{-/-}$ and wildtype mice. (B) Dimensional reduction (Umap) representation of combined measured cells with assigned cell types. (C) Cell interaction analysis of *Schlafenlnc*$^{-/-}$ and wildtype mice (*Cd45*+ cells from blood and heart) after TAC using CellChat[74]. (D) Differential signaling in *Schlafenlnc*$^{-/-}$ and WT macrophage and monocyte populations after TAC. Light grey and orange highlighted pathways are significantly enriched in wildtype or *Schlafenlnc*$^{-/-}$, respectively (p-val<0.05). (E) RNA Velocity of *Schlafenlnc*$^{-/-}$ and WT cells from heart after 6 days of TAC. Shown are macrophage and monocyte cell clusters. (F) Comparison of de-regulated genes (q-val<0.05) in TAC vs. basal condition in WT compared to de-regulated genes after 6d TAC KO

992 vs. WT in *Lyve1*$^{+}$ macrophages (G) Gene ontology terms of genes de-regulated in *SchlafenInc*-deficient
993 mice and after 6 days TAC.

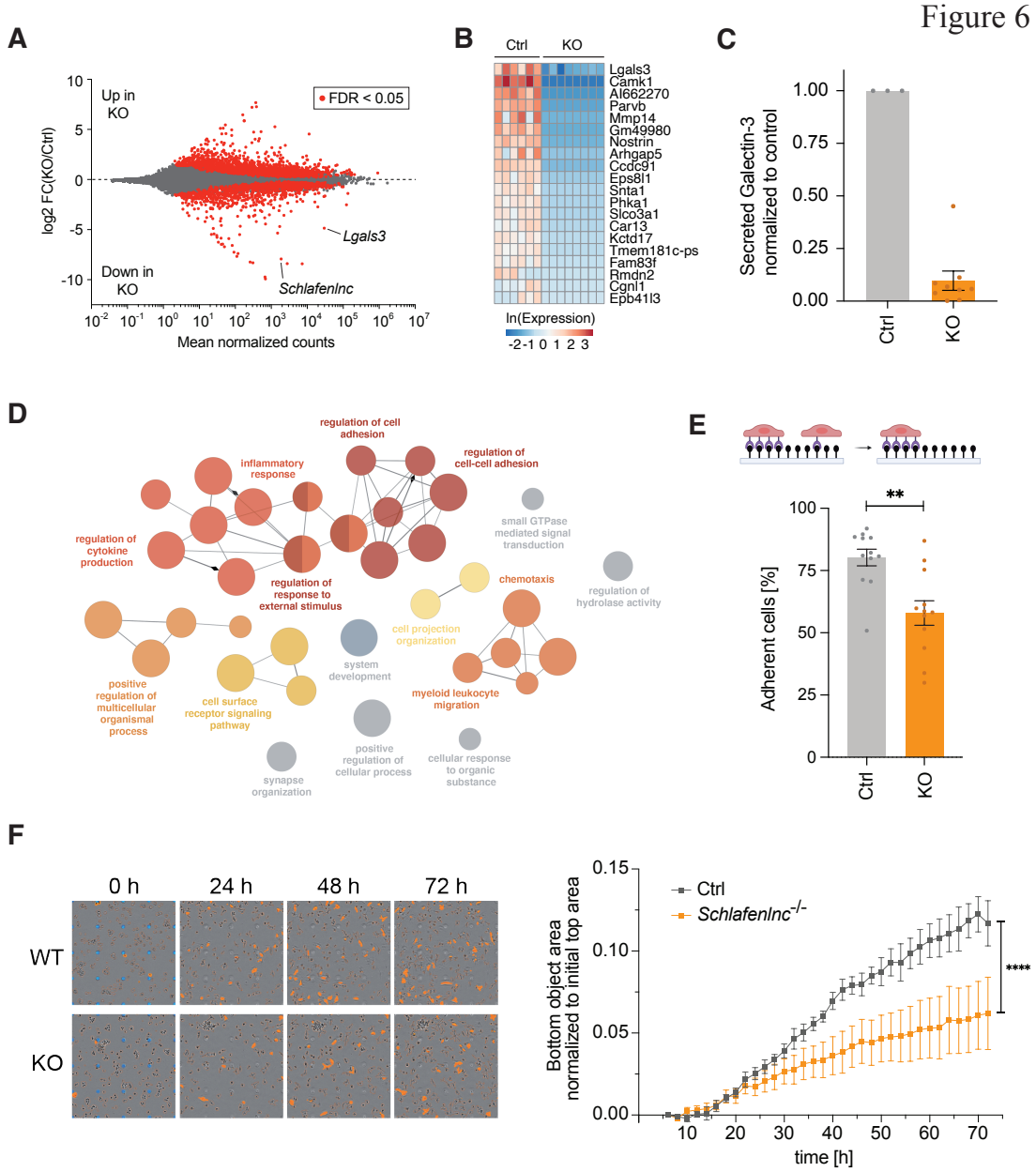

Figure 6: *Schlafenlnc* is required for the activation of macrophage gene programs for cell adhesion and migration.

(A) MA plot showing differentially expressed genes in *Schlafenlnc*$^{-/-}$ vs. Ctrl macrophages. Significantly deregulated genes (FDR < 0.05) are shown in red. (B) Heatmap of an unsupervised clustering showing the top 20 downregulated genes in *Schlafenlnc*$^{-/-}$ macrophages. (C) Measurement of Galectin-3 protein secretion by control and *Schlafenlnc*$^{-/-}$ macrophages as determined by ELISA. The supernatant of one control cell line and three *Schlafenlnc*$^{-/-}$ clones were used in n=3 independent experiments. Data points are displayed as mean ±SEM. (D) Functionally grouped gene ontology term analysis of biological processes associated with significantly downregulated genes (FDR < 0.05, log2FC < -1) in *Schlafenlnc*$^{-/-}$ macrophages. (E) Adhesion assay with control and *Schlafenlnc*$^{-/-}$ macrophages (Ctrl clones n=2, KO clones n=3; 4 independent experiments). Data points are displayed as mean ±SEM. (F) Chemotaxis assay against a gradient of the chemokine C5a with control and *Schlafenlnc*$^{-/-}$ macrophages

1007 stimulated with 10ng/ml LPS overnight (Ctrl clones n=1, KO clones n=3; 3 independent experiments).
1008 Data points are displayed as mean ±SEM.